Journal for ImmunoTherapy of Cancer

Natural lung-tropic T$_H$9 cells: a sharp weapon for established lung metastases

Tao Chen [iD],[1,2,3] Chenxiao Qiao,[4] Eloy Yinwang,[1,2,3] Shengdong Wang,[1,2,3] Xuehuan Wen,[5] Yixuan Feng,[6,7] Xiangang Jin,[8] Shuming Li,[9] Yucheng Xue,[1,2,3] Hao Zhou,[1,2,3] Wenkan Zhang,[1,2,3] Xianchang Zeng,[10] Zenan Wang,[1,2,3] Hangxiang Sun,[1,2,3] Lifeng Jiang,[1,2,3] Hengyuan Li,[1,2,3] Binghao Li,[1,2,3] Zhijian Cai,[1,10] Zhaoming Ye,[1,2,3] Nong Lin[1,2,3]

Correspondence to
Professor Nong Lin;
linnong@zju.edu.cn

Dr Zhaoming Ye;
yezhaoming@zju.edu.cn

Professor Zhijian Cai;
caizj@zju.edu.cn

Dr Binghao Li;
libinghao@zju.edu.cn

ABSTRACT

Background Lung metastasis remains the primary cause of tumor-related mortality, with limited treatment options and unsatisfactory efficacy. In preclinical studies, T helper 9 (T$_H$9) cells have shown promise in treating solid tumors. However, it is unclear whether T$_H$9 cells can tackle more challenging situations, such as established lung metastases. Moreover, comprehensive exploration into the nuanced biological attributes of T$_H$9 cells is imperative to further unravel their therapeutic potential.

Methods We adoptively transferred T$_H$1, T$_H$9, and T$_H$17 cells into subcutaneous, *in situ*, and established lung metastases models of osteosarcoma and triple-negative breast cancer, respectively, comparing their therapeutic efficacy within each distinct model. We employed flow cytometry and an *in vivo* imaging system to evaluate the accumulation patterns of T$_H$1, T$_H$9, and T$_H$17 cells in the lungs after transfusion. We conducted bulk RNA sequencing on *in vitro* differentiated T$_H$9 cells to elucidate the chemokine receptor CXCR4, which governs their heightened pulmonary tropism relative to T$_H$1 and T$_H$17 cell counterparts. Using Cd4^{cre} Cxcr4$^{flox/flox}$ mice, we investigate the effects of CXCR4 on the lung tropism of T$_H$9 cells. We performed mass spectrometry to identify the E3 ligase responsible for CXCR4 ubiquitination and elucidated the mechanism governing CXCR4 expression within T$_H$9 cellular milieu. Ultimately, we analyzed the tumor immune composition after T$_H$9 cell transfusion and evaluated the therapeutic efficacy of adjunctive anti-programmed cell death protein-1 (PD-1) therapy in conjunction with T$_H$9 cells.

Results In this study, we provide evidence that T$_H$9 cells exhibit higher lung tropism than T$_H$1 and T$_H$17 cells, thereby exhibiting exceptional efficacy in combating established lung metastases. CXCR4-CXCL12 axis is responsible for lung tropism of T$_H$9 cells as ablating CXCR4 in CD4$^+$ T cells reverses their lung accumulation. Mechanistically, tumor necrosis factor receptor-associated factor 6 (TRAF6)-driven hyperactivation of NF-κB signaling in T$_H$9 cells inhibited ITCH-mediated ubiquitination of CXCR4, resulting in increased CXCR4 accumulation and enhanced lung tropism of T$_H$9 cells. Besides, T$_H$9 cells' transfusion significantly improved the immunosuppressed microenvironment. T$_H$9 cells and anti-PD-1 exhibit synergistic effects in tumor control.

Conclusions Our findings emphasized the innate lung tropism of T$_H$9 cells driven by the activation of TRAF6,

WHAT IS ALREADY KNOWN ON THIS TOPIC

⇒ Mounting evidence suggests that T helper 9 (T$_H$9) cells possess remarkable capabilities in eliminating advanced tumors, especially in melanomas. T$_H$9 cells enhance antitumor immunity by supporting mast cell activation, promoting CC motif chemokine receptor 6$^+$ dendritic cell activation and recruitment, boosting cytotoxic T lymphocyte responses, enhancing natural killer cell function, and directly inducing tumor cell death.

WHAT THIS STUDY ADDS

⇒ In this study we reported the innate lung tropism of T$_H$9 cells contributes to its superior antitumor effects as compared with T$_H$1 and T$_H$17 cells in established lung metastases. Mechanistically, TRAF6-driven hyperactivation of NF-κB signaling in T$_H$9 cells inhibited ITCH-mediated ubiquitination of CXCR4, resulting in increased CXCR4 accumulation and enhanced lung tropism of T$_H$9 cells.

HOW THIS STUDY MIGHT AFFECT RESEARCH, PRACTICE OR POLICY

⇒ This study enriches biological characteristics of T$_H$9 cells and broaden the strategy for adoptive T cell therapy targeting established lung metastases of solid tumors.

which supports the potential of T$_H$9 cells as a promising therapy for established lung metastases.

BACKGROUND

Due to the distinctive pulmonary microenvironment, the lungs are frequently identified as a primary site for metastasis in a wide range of malignant tumors,[1] encompassing breast cancer, osteosarcoma (OS), prostate cancer, colorectal cancer, and other types. Despite the numerous and increasingly effective therapies for localized tumors, the prognosis for patients with established lung metastases remains highly problematic.[2] The treatment of lung metastasis poses significant challenges due to various factors. First, established lung

metastases typically indicate an advanced stage of cancer where the primary tumor has already spread to other distant sites. This advanced stage often results in a more aggressive and complex disease presentation. Second, the complexity of lung metastasis management extends to the limited treatment options available. Lung metastasis is known to exhibit resistance to conventional cancer treatments such as chemotherapy and radiation therapy.[3] Cancer cells that have metastasized to the lungs can acquire genetic alterations and develop resistance mechanisms, limiting the effectiveness of standard treatment approaches.[4 5] Although targeted therapies and immunotherapies have shown promise in certain solid tumors, their applicability depends on the tumor's specific molecular characteristics and the availability of suitable targeted agents.[6–9] Thus, there is still an urgent need to find novel strategies to improve the prognosis of patients with established lung metastases.

T helper 9 (T_H9) cells were first identified by Veldhoen and Dardalhon with the priority of secreting interleukin (IL)-9 and IL-10[10 11] and related to the development of many autoimmune diseases.[12–15] In addition to the proinflammatory ability, T_H9 cells exhibit superior efficacy in inhibiting the growth and metastasis of diverse solid tumors compared with T_H1 or T_H17 cells.[16–22] These results suggest the potential of T_H9 cells as potent T cells for cancer-adoptive cell therapy. Although studies have evaluated the therapeutic efficacy of T_H9 cells against cold tumors such as triple-negative breast cancer (TNBC) and OS, which supports the potential clinical application of T_H9-based adoptive cell therapy, the antitumor activity of T_H9 cells has been primarily investigated in melanoma.[23–25] Additionally, the protumor effect of T_H9 cells was also reported in lung cancer.[26 27] Therefore, the multifaceted role of T_H9 cells remains to be further elucidated.

In the current study, we first tested the antitumor effects of T_H9 cells against OS and TNBC in different models. Our results showed that T_H9 cells, compared with T_H1 and T_H17 cells, exhibit superior antitumor efficacy toward the established lung metastases model but not the subcutaneous and primary model. We demonstrated this was associated with the innate lung affinity of T_H9 cells driven by the CXCR4-CXCL12 chemoattraction axis. Further experiments proved that tumor necrosis factor (TNF) receptor-associated factor 6 (TRAF6)-mediated activation of NF-κB signaling in T_H9 cells led to the phosphorylation of inhibitor of nuclear factor kappa B kinases (IKKs), which inhibited the activity of E3 ubiquitination ligase ITCH, resulting in the attenuated ubiquitination of CXCR4 in T_H9 cells. T_H9 cells can enhance the proportion of immune cell subsets *via* IL-9, resulting in a reshaped tumor microenvironment at lung tumor sites. Infusion of T_H9 cells increases the number of $CD8^+T$ cells at tumor sites, and combining T_H9 cells therapy and anti-programmed cell death protein-1 (PD-1) enhances antitumor effects against established lung metastases.

METHODS
Sex as a biological variable
Our study exclusively examined female mice. It is unknown whether the findings are relevant for male mice.

Human samples
Patients diagnosed with OS lung metastasis between September 2016 and December 2022 at the Musculoskeletal Tumor Center of the Department of Orthopedics at The Second Affiliated Hospital of Zhejiang University School of Medicine were recruited to this study for immunohistochemistry analysis. In total, 22 cases of formalin-fixed, paraffin-embedded tissue blocks of OS lung metastasis were included. Experienced specialists performed all surgeries. All the patients were informed of the usage of their tissue samples.

Mice and cell lines
BALB/C (5–8 week-old) mice were purchased from SLAC (Shanghai, China). The Institutional Animal Care and Use Committee approved all animal studies. DO11.10 mice were donated by Dr Fang Zhang (Medical School of Nanjing University, Nanjing, China). CD45.1 mice were bred by ourselves. *Cxcr4^{flox/flox}* mice were bought from Cyagen Biosciences (Suzhou, Jiangsu Province, China) and then crossed with *Cd4^{cre}* mice to produce *Cd4^{cre} Cxcr4^{flox/flox}* mice. Mice were housed in a specific pathogen-free facility, and experimental protocols were approved by the Animal Care and Use Committee of the School of Medicine, Zhejiang University (Ethical approval number: 26253).

There were three to five animals in each group. Five animals of the same group live in a single animal cage. The sample size was determined based on the number of experimental groups and different time points of analysis. The experiments were conducted in a random manner. In each experiment, mice of the same sex and age were randomly divided into different groups. After allocation, each group comprised an equal number of animals with comparable weights, aiming to minimize experimental error. No criteria were set for including or excluding animals. No data points were excluded from the analysis.

Murine K7M2 and 4T1 cells were obtained from the Cell Bank of Shanghai Institute of Biochemistry and Cell Biology, Chinese Academy of Sciences (Shanghai, China). The K7M2-ovalbumin (OVA) cells, K7M2-Luci-OVA cells, 4T1-OVA cells and 4T1-Luci-OVA cells were transfected with lentiviral transfection in our laboratory. K7M2-OVA cells, K7M2-Luci-OVA cells, 4T1-OVA cells and 4T1-Luci-OVA cells were cultured in Dulbecco's Modified Eagle's Medium supplemented with 10% fetal bovine serum (Invitrogen, Carlsbad, California, USA), and 1% penicillin/streptomycin. Cells were maintained at 37°C in 5% CO_2. All cells were routinely tested for mycoplasma contamination using the Mycoplasma Detection Kit (ab289834, Abcam, Cambridge, Massachusetts, USA) and were found to be negative.

Tumor growth experiments

For K7M2 lung OS and 4T1 lung breast cancer models, mice were injected intravenously with 1×10^5 4T1-OVA-luci or K7M2-OVA-luci in 100 μl of phosphate-buffered saline (PBS) (P1010, Solarbio, Beijing, China). Mice were transferred with 3×10^6 OVA-specific T_H1, T_H9, or T_H17 cells resuspended in 100 μl PBS intravenously on day 5, day 12 and day 19. At day 7, day 14 and day 21, mice were anesthetized with 1% pentobarbital sodium and injected intraperitoneally with luciferin (P1043, Promega, Madison, Wisconsin, USA) at 100 μg kg^{-1} of mice weight. After 10 min of luciferin injection, images were acquired with the IVIS Spectrum In Vivo Imaging System (Perkin-Elmer, Waltham, Massachusetts, USA). Total photon flux in the lung area was analyzed with Living Image software (PerkinElmer).

For the subcutaneous tumor model, mice were injected with 1×10^6 4T1 OVA or K7M2-OVA cells in 100 μl of PBS subcutaneously. For the primary tumor model, mice were injected into the mammary fat pad of the mice with 1×10^6 4T1 OVA or injected into the bone marrow cavity of the mouse tibia with 1×10^6 K7M2-OVA cells in 20 μl of PBS. Tumor volume was monitored by caliper every other day after 7 days of injection and calculated by the formula $V=a\times b^2/2$ (a: the maximal diameter of the tumor, b: the minimal diameter).

In subcutaneous and primary tumor models, mice were transferred with 3×10^6 OVA-specific T_H1, T_H9, or T_H17 cells resuspended in 100 μl PBS intravenously on day 7 and day 14. For *in vivo* blockade of IL-9, individual mice were injected with 100 μg *InVivo*Mab anti-mouse IL-9 (BE0181, clone: 9C1, Bio X Cell, West Lebanon, New Hampshire, USA) intraperitoneally every 2 days since the same day of tumor inoculation. To eliminate CD8$^+$ T cells *in vivo*, individual mice received 40 μg anti-CD8 (BE0061, clone: 2.43, Bio X Cell) *via* intraperitoneal injection every 2 days since the same day of tumor inoculation. For *in vivo* blockade of PD-1, individual mice were injected with 100 μg *InVivo*Mab anti-mouse PD-1 (BE0146, clone: RMP1-14, Bio X Cell, West Lebanon, New Hampshire, USA) intraperitoneally every 2 days since the same day of tumor inoculation. According to the criteria of the Animal Care and Use Committee of the School of Medicine, Zhejiang University, when the tumor size was over 2000 mm^3, the tumor-bearing mice were euthanized by an intraperitoneal injection of 50 mg kg^{-1} pentobarbital sodium.

Transfer of CD45.1-T_H cells subsets into CD45.2 mice

CD45.1-naïve CD4$^+$ T cells were generated from CD45.1 mice and *in vitro* polarized to CD45.1-T_H1, T_H9 and T_H17 cells under polarization condition medium for 4 days. In some experiments, 1×10^7 CD45.1-T_H9 cells were intravenously transferred into CD45.2 mice in 100 μl PBS. 48 hours later, CD45.2 mice were sacrificed, and the percentage of CD45.1$^+$ T cells in the lung, liver, spleen, bone marrow and lymph node were analyzed by flow cytometry. In some experiments, 1×10^6 CD45.1-T_H1, T_H9 and T_H17 cells were intravenously transferred into CD45.2 mice in 100 μl PBS. 48 hours later, CD45.2 mice were sacrificed, and the percentage of CD45.1$^+$ T cells in the lung was analyzed by flow cytometry.

In some experiments, individual mice were intraperitoneally injected with 1 mg kg^{-1} ML339 (HY-122197), 1 mg kg^{-1} C-021 (HY-103364), 1 mg kg^{-1} R243 (HY-122219) or 1 mg kg^{-1} AMD3100 (HY-10046) in 100 μl PBS 1 day before transfer of T_H cell subsets. The inhibitors were all purchased from MCE (New Jersey, USA).

In vitro CD4$^+$ T cell culture

Naïve CD4$^+$ CD62L$^+$ cells were isolated using EasySep Mouse CD4$^+$ T Cell Isolation Kit (19852, STEMCELL Technologies, Vancouver, BC, V6A 1B6, Canada) and EasySep Mouse Biotin Positive Selection Kit II (17665, STEMCELL Technologies). Naïve CD4$^+$ T cells were seeded into 48-well plates with plate-bound anti-CD3 (BE0001-1, 2 μg mL^{-1}, Bio X Cell) and anti-CD28 (BE0015-5, 2 μg mL^{-1}, Bio X Cell). 1×10^6 cells per well, and polarized into effector CD4$^+$ T lymphocyte subsets for 4 days without cytokines, and with anti-IFN-γ (BE0054, 10 μg mL^{-1}, Bio X cell) and anti-IL-4 (BE0045, 10 μg mL^{-1}, Bio X cell) (T_H0 cells); with IL-12 (130-096-707, 20 ng mL^{-1}, Miltenyi Biotec, Bergisch Gladbach, Germany) and anti-IL-4 (10 μg mL^{-1}) for T_H1 cells; with TGF-β1 (130-095-067, 2 ng mL^{-1}, Miltenyi Biotec), IL-4 (20 ng mL^{-1}), and anti-IFN-γ (10 μg mL^{-1}) for T_H9 cells; with TGF-β1 (2 ng mL^{-1}), IL-6 (130-094-065, 25 ng mL^{-1}, Miltenyi Biotec), anti-IFN-γ (10 μg mL^{-1}), and anti-IL-4 (10 μg mL^{-1}) for T_H17 cells.

In vivo fluorescence imaging

For the T cell homing experiment, T cells stained by 1,1-dioctadecyl-3,3,3,3 tetramethylindotricarbocyaine iodide (DiR) (5 μM, Caliper Life Sciences, Boston, USA) for 20 min at 37°C. After being thoroughly washed in PBS three times, 3×10^6 T cells were delivered intravenously in 100 μl PBS. IVIS Spectrum Animal Imaging System was used to evaluate the homing ability of T cells 48 hours after T cells transfusion.

In vitro tumor-specific cytotoxicity of T_H1, T_H9 and T_H17 cells

OVA-specific naïve CD4$^+$ T cells were generated from OVA-specific DO11.10 mice and *in vitro* polarized to OVA-specific T_H1, T_H9 and T_H17 cells under polarization condition medium for 4 days. K7M2-OVA or 4T1-OVA and K7M2-wild-type (WT) or 4T1-WT tumor cells were labeled with CFSE (Thermo Fisher Scientific, Waltham, California, USA). K7M2-OVA or 4T1-OVA cells were labeled with 5 μM CFSE (CFSE^{high}), while K7M2-WT or 4T1-WT cells were labeled with 0.5 μM CFSE (CFSE^{low}) for 10 min at 37°C. Then the tumor cells were mixed at a 1:1 ratio and seeded into 96-well plates (5×10^4 cells/well; 2.5×10^4 K7M2-OVA cells and 2.5×10^4 K7M2-WT cells; 2.5×10^4 4T1-OVA cells and 2.5×10^4 4T1-WT cells). OVA-specific T_H1, T_H9 and T_H17 cells (5×10^5) were added and incubated for 24 hours. A mixture of tumor cells cultured alone was regarded as the control. 24 hours later, the cells

were collected and stained by Fixable Viability Dye (FVD) eFluor™ 780 and CD4 antibodies to dissect the surviving tumor cells (FVD⁻ CD4⁻ CFSE⁺) and detected by flow cytometry. Ratio = % (CFSE^{hi}) peak/% (CFSE^{lo}) peak. Tumor-specific lysis = (1−(Control ratio/Experimental ratio)) × 100.

Flow cytometry

Intranuclear staining was carried out with fixation/permeabilization buffer solution (00-5123-43 and 00-5223-56, eBioscience, San Diego, California, USA). For intracellular staining, cells were stimulated for 4 hours at 37°C in a medium containing PMA (P1585, 50 ng mL^{-1}, Sigma-Aldrich, St Louis, Missouri, USA), ionomycin (I3909, 1 µg mL^{-1}, Sigma-Aldrich), and brefeldin A solution (00-4506-51, eBioscience, California, USA). Then, the cells were subjected to an intracellular staining protocol (00-8222-49, eBioscience) and the stained cells were analyzed using ACEA NovoCyte (Agilent Technologies, California, USA). Data were analyzed using NovoExpress (Agilent Technologies).

Transwell migration assay

Transwell chambers with microporous membranes of 4 µm pore-size (Corning, New York, USA) were used to evaluate the migration ability of T_H0, T_H1, T_H9 and T_H17 cells in response to different organ lysates and CXCL12. Briefly, $5×10^5$ differentiated T_H cells were seeded onto the upper chamber, and organ lysates or CXCL12 at 100 ng µl^{-1} were added to the lower chamber. After 4 hours, the cells in the lower chamber were collected and counted by flow cytometry. In some experiments, T_H9 cells were pretreated with AMD3100 (5 µg/mL) for 24 hours. Migration index was calculated as the ratio of migrated cells in the presence and absence of organ lysates or CXCL12. Each experiment was done in triplicate.

Real-time PCR

Total RNA was extracted from cells using RNAiso Plus (9109, Takara Biomedical Technology, Beijing, China) and reverse transcribed into complementary DNA (cDNA) with a HiFiScript cDNA Synthesis Kit (CW2569, Cowin Biotech, Beijing, China) according to the manufacturer's instructions. RT-PCR was performed by ChamQ Universal SYBR qPCR Master Mix (Q711-02, Vazyme, Nanjing, Jiangsu, China) and specific primers in the applied Bio-Rad real-time PCR system. The following thermal cycling conditions were used for PCR: 1 cycle at 95°C for 30 s, followed by 40 cycles at 95°C for 5 s and 60°C for 34 s. The data were analyzed by the $2^{-\Delta\Delta Ct}$ method.

Immunofluorescent

T_H0, T_H1, T_H9 and T_H17 cells were collected and fixed with 4% paraformaldehyde for 30 min and permeabilized with 0.1% Triton X-100 for 10 min. Then, the cells were blocked with 3% bovine serum albumin and 5% goat serum and incubated with anti-CXCR4 (sc-53534, Santa Cruz, Santa Cruz, California, USA) at 4°C overnight. The next day, cells were stained with iFluor 594 Conjugated Goat anti-mouse immunoglobulin G Goat Polyclonal Antibody (HA1126, HUABIO, Hangzhou, Zhejiang, China). Nuclei were stained with 4'6-diamidino-2-phenylindole (DAPI) (H-1900–10, Vectorlabs, San Francisco, USA).

For lung tissue section staining, the lungs were dissected and fixed overnight with 4% paraformaldehyde and 20% sucrose. The lungs were cut into 8-µm-thick sections for immunofluorescence staining and applied to glass slides. After being fixed and stained with DAPI (D9542, Sigma-Aldrich), the sections were washed with PBS and examined with an Olympus IX83-FV3000 confocal microscope (Olympus Corp, Tokyo, Japan).

Western blotting

Cells were collected and washed with 1 mL cold PBS three times. Then, the cells were lysed on ice in Radio-immunoprecipitation assay buffer (RIPA) lysis buffer (P0013B, Beyotime Biotechnology, Shanghai, China) for 30 min. Subsequently, the cell lysates were separated by sodium dodecyl sulfate-polyacrylamide gel electrophoresis on 10% or 12% gels and were transferred onto polyvinylidene difluoride membranes. The membranes were blocked with 5% bovine serum albumin (BSA) in phosphate buffered solution (PBST) buffer and were incubated with primary antibodies overnight at 4°C. After washing three times, the membranes were incubated with secondary antibodies at room temperature for 1 hour. Each membrane was scanned by a Tanon 4500 imaging system (Shanghai, China).

Immunoprecipitation

T_H0, T_H1, T_H9 and T_H17 cells were collected and washed three times with cold PBS. Cell extracts were prepared on ice for 30 min using lysis buffer containing 50 mM Tris (pH 7.4), 150 mM NaCl, 0.5% (vol/vol) Nonidet P-40, and 1 mM EDTA supplemented with protease inhibitor cocktail. Lysates were incubated with indicated antibody-coupled beads at 4°C overnight. Immunoprecipitates were washed three times with lysis buffer and subjected to a western blotting assay.

Mass spectrometry

Each pulldown sample was run just in the separation gel and was cut into approximately 1-mm³ pieces, then subjected to in-gel trypsin digestion and dried. Samples were reconstituted in 5 µl of high-performance liquid chromatography solvent A (2.5% acetonitrile and 0.1% formic acid). A nanoscale reverse-phase high-performance liquid chromatography capillary column was created by packing 5-µm C18 spherical silica beads into a fused silica capillary (100 µm inner diameter × ~20 cm length) using a flame-drawn tip. After the column was equilibrated, each sample was loaded onto the column using an autosampler. A gradient was formed, and peptides were eluted with increasing concentrations of solvent B (97.5% acetonitrile and 0.1% formic acid). As the peptides eluted, they were subjected to mass spectrometry (MS), as described above. MS analysis of the protein content was performed

Small interference RNA transfection

Naive CD4+ T cells were seeded into 6-well plates at 5×10^6 per well. Then, the cells were transfected with scramble negative control or targeted small interference RNA using TransIT-TKO Transfection Reagent (Mirus Bio, Madison, Wisconsin, USA) according to the manufacturer's instructions.

Retroviral infection of CD4+ T cells

Retroviruses were produced by transfecting Plat-E cells with 7.5 µg of pMX-*Ires-gfp* or pMX-*Itch-gfp*. The cell culture medium was replaced with fresh medium after 10 hours, and the retrovirus-containing supernatant was collected after an additional 72 hours. Naïve CD4+ T cells were first stimulated with anti-CD3 and anti-CD28 antibodies. At the 24 hours and 36 hours time points, activated T cells were infected with 500 µl of the viral supernatant for 1 hour by centrifugation at 1500×g in the presence of 10 µg ml⁻¹ polybrene and incubated at 37°C for an additional 1 hour before removal from the viral supernatant and resuspension in the corresponding T cell medium for 72 hours.

Isolation of tumor-infiltrating lymphocytes

Tumors were dissected and subjected to enzymatic digestion with 1 mg mL⁻¹ collagenase IV (CLS-4, Worthington Biochemical Freehold, New Jersey, USA) and 0.5 mg mL⁻¹ DNase I (DN25, Sigma-Aldrich) at 37°C for 90 min followed by Percoll (GE Healthcare, Uppsala, Sweden) gradient purification.

Measurement of cytokine levels

Lung homogenates were assayed by ELISA to measure the levels of CXCL1, CXCL12, CXCL14, CXCL15 and CXCL16 according to the manufacturer's instructions. ELISA kits for murine CXCL1 (RK0038), CXCL12 (RK00168), CXCL14 (RK02643), CXCL15 (RK07476) and CXCL16 (RK00417) were all purchased from ABclonal (Wuhan, Hubei, China). Absorbance values were measured with a SynergyMx M5 microplate reader (Molecular Devices, Silicon Valley, California, USA).

Statistical analysis

All data are expressed as the mean±SEM. Statistical analyses were performed with GraphPad Prism V.7.0 software. All the data were performed the Shapiro-Wilk test to confirm their distribution. For the normally distributed data, unpaired Student's t-test analyzed the differences between two groups of data, and differences among three or more groups were analyzed by one-way analysis of variance (ANOVA) or two-way ANOVA followed by a post hoc Tukey test. For the non-normally distributed data, the Mann-Whitney test was used for means comparison between the two groups. The Kruskal-Wallis test was used for the means comparison of multiple individual data sets. Overall survival was assessed by Kaplan-Meier analysis.

The Spearman's rank-order correlation test was used for Pearson's correlation analysis. A value of $p < 0.05$ was considered statistically significant. The sample size ranges from 3 to 5 according to the effect of a 50% increase and 25% SD compared with the control group. The acceptable error rate is 5%.

RESULTS

### T$_H$9 cells have therapeutic advantages toward established lung metastases

T$_H$9 cells exhibited more substantial antitumor effects than T$_H$1 and T$_H$17 cells in some solid tumors.[16 21 22 28] However, the antitumor effects of T$_H$9 cells are primarily evaluated in melanoma and lung adenocarcinoma.[29 30] To validate whether T$_H$9 cells are also effective in tumors with poor immune infiltration, such as OS and TNBC, we assessed the antitumor effects of tumor-specific T$_H$1, T$_H$9 and T$_H$17 cells in different mouse models of OS and TNBC. OVA-specific T$_H$1, T$_H$9 and T$_H$17 cells were generated by priming DO11.10 mice derived naïve CD4+ CD62L+ T cells in the corresponding polarized conditions for 4 days (online supplemental figure S1A). Then, we transferred tumor-specific T$_H$1, T$_H$9 or T$_H$17 cells into Balb/c mice bearing K7M2-OVA cells or 4T1-OVA cells, respectively. Although T$_H$1, T$_H$9 and T$_H$17 cell transfusion all resulted in partial tumor inhibition in the subcutaneous models, T$_H$9 cells failed to induce stronger tumor eradication as reported in melanoma[16 22] (online supplemental figure S1B,C). T$_H$1, T$_H$9 and T$_H$17 cells consistently extended the survival time of tumor-bearing mice, but T$_H$9 cells showed no priority relative to T$_H$1 and T$_H$17 cells (online supplemental figure S1D). Similarly, we found that the tumor-inhibiting ability of T$_H$9 cells was not better than T$_H$1 and T$_H$17 cells in the primary models of OS and TNBC (online supplemental figure S1E–G). We also tested the control of tumor growth by different T$_H$ cell subsets in the setting of established lung metastases (figure 1A). However, we observed that T$_H$9 cells exhibited stronger antitumor effects against pulmonary OS and TNBC than T$_H$1 and T$_H$17 cells. (Figure 1B,C). Besides, T$_H$9 cells further prolonged the survival period of lung tumor-bearing mice (figure 1D). The H&E staining also proved lesser pulmonary tumor burden after T$_H$9 cells treatment as compared with T$_H$1 and T$_H$17 cells (figure 1E,F). Therefore, our results indicate that T$_H$9 cells have a superior therapeutic effect on lung metastatic lesions of OS and TNBC than T$_H$1 and T$_H$17 cells.

T$_H$9 cells possess unique lung tissue affinity

We initially hypothesized that this difference could be attributed to the distinct direct cytotoxic abilities of different T$_H$ cell types against tumor cells, as existing literature has reported on the direct killing capability of T$_H$9 cells.[21 22] Thus, we first test the tumor-specific killing ability of T$_H$1, T$_H$9 and T$_H$17 cells toward K7M2 and 4T1 cells *in vitro*. According to our results, T$_H$1, T$_H$9 and T$_H$17 cells seemed to promote rather than inhibit the growth of
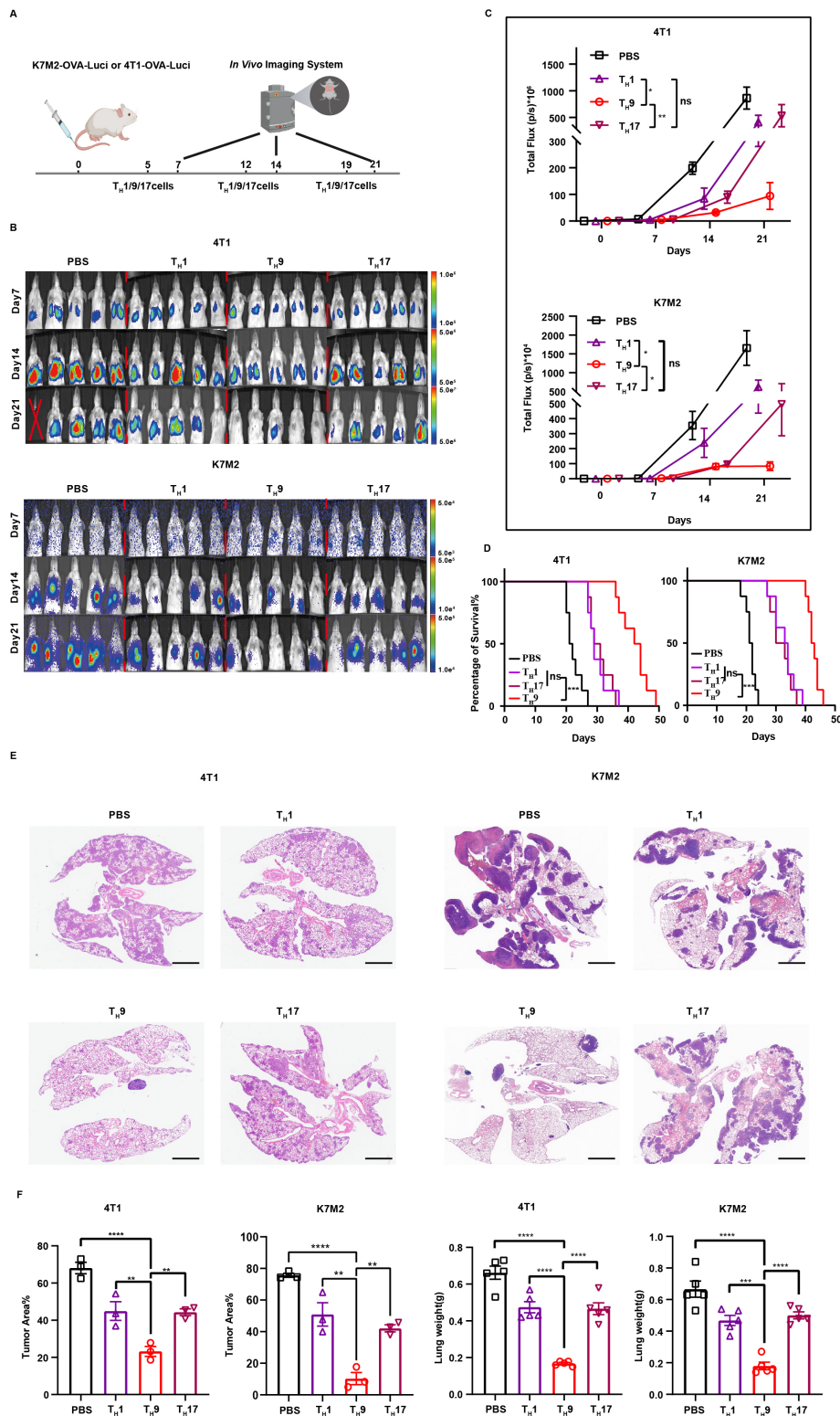
Figure 1 T$_H$9 cells exhibited superior antitumor effects in established lung metastasis as compared with T$_H$1 and T$_H$17 cells. (A) Balb/c mice were inoculated with 1×10^5 4T1-OVA-luci or K7M2-OVA-luci in 100 µl PBS intravenously on day 0. Tumor-bearing mice were transferred with 3×10^6 OVA-specific T$_H$1, T$_H$9, or T$_H$17 cells in 100 µl PBS intravenously on day 5, day 12 and day 19. (B and C) *In vivo* bioluminescence images (B) and quantification (C) of the tumor burden in lungs on day 7, day 14 and day 21. (D) Survival of K7M2-OVA or 4T1-OVA tumor-bearing mice with lung metastasis treated with PBS, tumor-specific T$_H$1, T$_H$9, and T$_H$17 cells. (E) H&E staining of lungs bearing with K7M2-OVA or 4T1-OVA tumor on day 14. Scale bar, 2.5 mm. (F) Tumor area and lung weight correspond to (E). Data were analyzed by one-way ANOVA test or unpaired t-test. Representative results from three independent experiments are shown (mean±SEM); n=5 in (B, C and F), n=8 in (D), n=3 in (E and F). ns denote no significant difference, *indicates $p<0.05$, **indicates $p<0.01$, ***indicates $p<0.001$, ****indicates $p<0.0001$. ANOVA, analysis of variance; OVA, ovalbumin; PBS, phosphate-buffered saline; T$_H$, T helper.

4T1 cells. Besides, T_H1 and T_H9 cells showed slight tumor-specific killing ability toward K7M2 cells with no significant difference, and T_H17 cells still promoted the growth of K7M2 cells (online supplemental figure S2A,B). These results indicated that T_H9 cells do not possess superior direct cytotoxicity toward tumor cells compared with T_H1 and T_H17 cells. Next, we speculated more T_H9 cells were accumulated in lung tissue than T_H1 and T_H17 cells since the distribution of T cells contributes to the antitumor effects. To prove our speculation, we labeled exogenous T_H cell subsets with DIR to trace the accumulation of T_H cells in lungs after adoptively transfusing them into mice with established lung metastases (figure 2A). As expected, higher amounts of T_H9 cells were accumulated in the lungs than T_H1 and T_H17 cells (figure 2B,C). To evaluate whether tumors affect the lung tropism of T_H9 cells, we explored the distribution of transferred T_H9 cells in multiple organs in tumor-free mice, including the lungs, liver, spleen, lymph nodes and bone marrow. We generated CD45.1-T_H9 cells *in vitro* and then intravenously transfused them into CD45.2 mice (figure 2D). We detected the distribution of CD45.1$^+$ cells in different organs through flow cytometry after 48 hours and found that most CD45.1-T_H9 cells were aggregated in lung tissues (figure 2E,F). Next, we compared the accumulation of T_H1, T_H9, and T_H17 cells in the lungs of tumor-free mice and found that T_H9 cells presented much higher lung tissue tropism than T_H1 and T_H17 cells (figure 2G,H). Consistent with these results, lung tissue lysates had a more vital ability to chemoattract T_H9 cells *in vitro* than liver and spleen lysates (figure 2I). Furthermore, lung tissue lysates specifically promoted the chemoattraction of T_H9 cells but not T_H1 and T_H17 cells (figure 2J). Altogether, these results suggested that T_H9 cells possess natural lung tropism.

Lung tropism of T_H9 cells depends on the CXCR4-CXCL12 chemokine axis

Since T_H9 cells were significantly attracted by lung lysates (figure 2I,J), we supposed there are probably high levels of chemokine(s) responsible for T_H9 cell chemotaxis in the lungs. We analyzed transcriptomic data from normal mouse lung tissues sourced from the GSE179554 data set to evaluate the basal expression levels of common chemokines. Our analysis revealed that *Cxcl15*, *Ccl6*, *Cxcl12*, *Cxcl14* and *Cxcl16* exhibited the highest basal expression (figure 3A). High levels of CXCL15, CXCL12, CXCL14 and CXCL16 proteins in the lungs were further confirmed (online supplemental figure S3A). Next, the global transcriptional profile of T_H0 and T_H9 cells were analyzed in triplicate to determine the upregulated chemokine receptors in T_H9 cells and revealed that the genes encoding chemokine receptors, including CC motif chemokine receptor 4 (*Ccr4*), *Ccr6*, *Ccr7*, *Ccr8*, *Cxcr4*, *Cxcr5* and *Cxcr6*, were upregulated in T_H9 cells (figure 3B). Then, we analyzed the messenger RNA (mRNA) levels of chemokine receptors in T_H9 cells as compared with T_H0 cells and revealed significant upregulation of *Ccr8* and *Ccr6*,

followed by *Cxcr4*, *Cxcr2* and *Cxcr1*. Whereas the expression levels of *Cxcr5* and *Cxcr6* in T_H9 cells did not exhibit significant upregulation compared with those in T_H0 cells (figure 3C). To compare the potential of different chemokine axes in the lung tropism of T_H9 cells more intuitively, we standardized the expression chemokines in lung tissues and the chemokine receptors on T_H9 cells and multiplied chemokines with paired chemokine receptors. Among all these paired chemokine-chemokine receptor axes, CXCL15 was ruled out since the corresponding receptor of CXCL15 was still elusive. In this way, we noticed that the CXCL12-CXCR4 axis ranked first, suggesting the potential to recruit T_H9 cells into the lungs (figure 3D). In addition, we confirmed the upregulated CXCL12 in lung tumor-bearing mice relative to tumor-free mice (online supplemental figure S3B).

Subsequently, we employed inhibitors ML339, C-021, R243, and AMD3100 to obstruct the chemokine–chemokine receptor axis in the lungs, targeting the CXCL16-CXCR6, CCL17-CCR4, CCL1-CCR8, and CXCL12-CXCR4 axes, respectively. We found that CXCR4 antagonist AMD3100 specifically inhibited T_H9 cell accumulation in the lungs, while other inhibitors had no obvious influence (figure 3E,F). Besides, AMD3100 did not impede the accumulation of T_H1 and T_H17 cells in the lungs (online supplemental figure S3C). Consistently, CXCR4 antagonist AMD3100 abolished the increased T_H9 rather than T_H1 and T_H17 cells chemoattraction induced by lung tissue lysates *in vitro* (figure 3G). To further confirm the role of the CXCL12-CXCR4 axis in T_H9 cells chemotaxis, recombinant CXCL12 protein was used to test the chemoattraction ability of T_H1, T_H9 and T_H17 cells. T_H9 cells were more susceptible to recombinant CXC12-induced chemoattraction than T_H1 and T_H17 cells (figure 3H). Altogether, these results suggested that the CXCL12-CXCR4 axis is central to T_H9 cell recruitment.

CXCL12 is a critical factor in both physiological and pathological processes, including embryogenesis, hematopoiesis, angiogenesis, and inflammation, as it activates and induces the migration of hematopoietic progenitor and stem cells, endothelial cells, and a majority of leukocytes. CXCL12 is predominantly expressed in the lungs, liver, and bone marrow.[31 32] In healthy tissues, CXCL12 is secreted by stromal cells, including fibroblasts, macrophages, and endothelial cells.[33 34] Considering the responsive difference between T_H cell subsets toward CXCL12, we wondered whether T_H9 cells express increased CXCR4 compared with T_H1 and T_H17 cells. Our results indicated that the total and surface CXCR4 levels of T_H9 cells were higher compared to other T_H cell subsets (figure 3I–L and online supplemental figure S3D). Furthermore, we constructed *Cd4^{Cre}Cxcr4$^{flox/flox}$* C57BL/6 mice and obtained *Cd4^{Cre}Cxcr4$^{flox/flox}$* -T_H9 cells (online supplemental figure S3E) . Compared with T_H9 cells differentiated from WT naïve CD4$^+$ T cells (*Cxcr4$^{flox/flox}$*-T_H9 cells), the accumulation of *Cd4^{Cre}Cxcr4$^{flox/flox}$* -T_H9 cells in lung tissues was significantly inhibited (figure 3M,N). Besides, the chemoattraction of lung lysate to T_H9 cells was also blunted
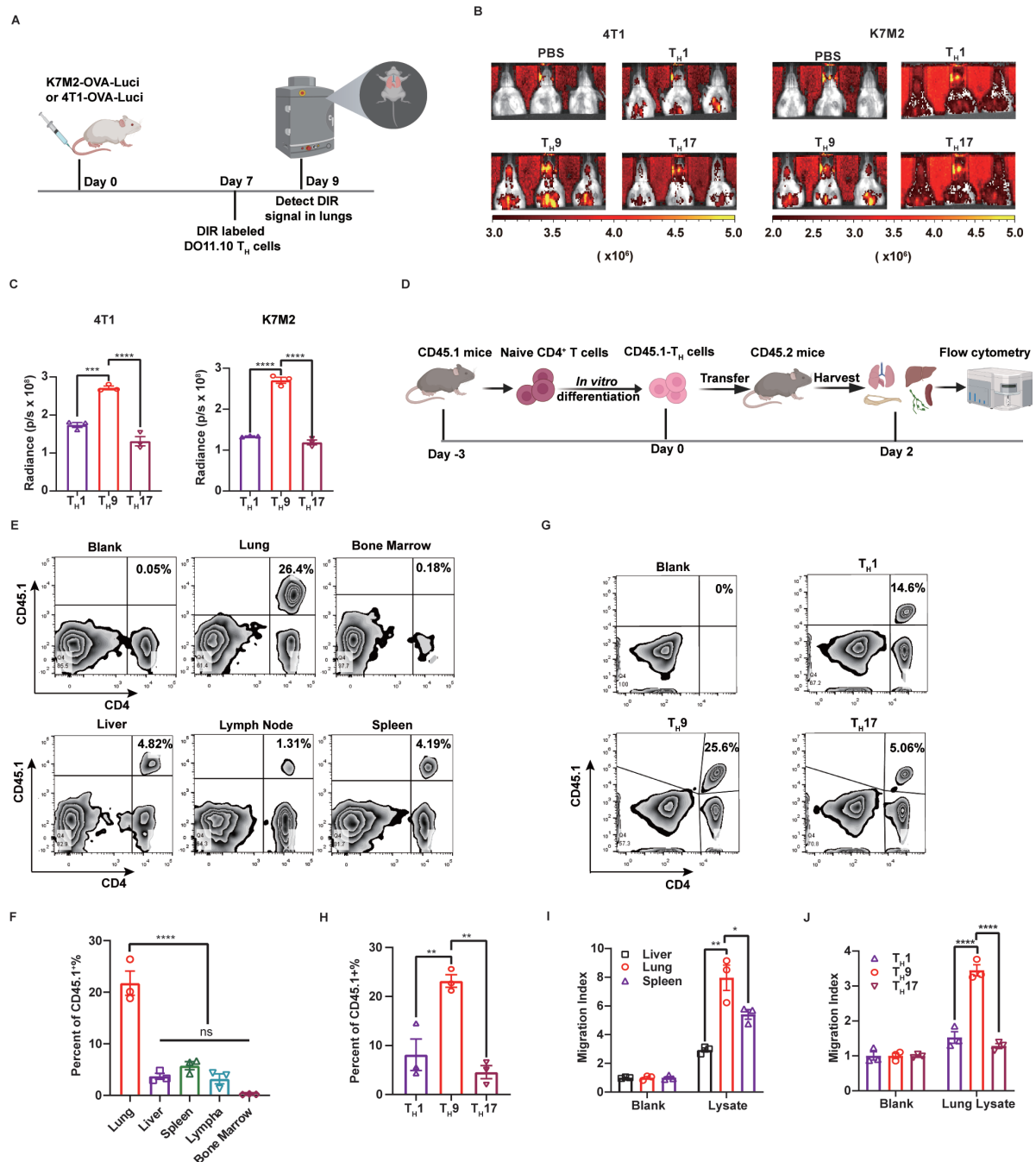
Figure 2 T$_H$9 cells show higher lung affinity as compared with T$_H$1 and T$_H$17 cells. (A) Balb/c mice were inoculated with 1×10^5 4T1-OVA-luci or K7M2-OVA-luci in 100 µl PBS intravenously on day 0. Tumor-bearing mice were transferred with 3×10^6 DIR labeled OVA-specific T$_H$1, T$_H$9, or T$_H$17 cells in 100 µl PBS intravenously on day 7. 2 days later, *in vivo* bioluminescence spectrum was used to detect the accumulation of transferred T$_H$ cells in lungs. (B and C) *In vivo* bioluminescence images (B) and quantification (C) of T$_H$ cell subsets accumulated in lungs 48 hours after transfusion of DIR labeled tumor-specific T$_H$1, T$_H$9, and T$_H$17 cells. (D) CD45.1$^+$ naïve CD4$^+$ T cells were derived from CD45.1$^+$ mice and differentiated into CD45.1$^+$-T$_H$ cells *in vitro* for 4 days. CD45.1$^+$-T$_H$ (1×10^7) were transferred intravenously into CD45.2$^+$ C57 mice. 48 hours later, the mice were sacrificed and the CD45.1$^+$-T$_H$ cells in different organs were detected by flow cytometry. (E and F) The representative density plot (E) and quantification (F) of CD45.1-T$_H$9 cells in lung, liver, spleen, lymphoma, and bone marrow 48 hours after intravenous injection of CD45.1 derived T$_H$9 cells into healthy CD45.2 mice. (G and H) The representative density plot (G) quantification (H) of CD45.1-T$_H$1, T$_H$9 and T$_H$17 cells in the lung 48 hours after intravenous injection of CD45.1 derived-T$_H$ cell subsets into healthy CD45.2 mice. (I) Migration index of T$_H$9 cells toward liver, lung, and spleen lysate (100 µg/mL) detected by transwell. (J) Migration index of T$_H$1, T$_H$9, and T$_H$17 cells toward lung lysate (100 µg/mL) detected by transwell. Data were analyzed by one-way ANOVA test or unpaired t-test. Representative results from three independent experiments are shown (mean±SEM); n=3 in all groups. ns denote no significant difference,*indicates $p<0.05$, **indicates $p<0.01$, ***indicates $p<0.001$, ****indicates $p<0.0001$. ANOVA, analysis of variance; DiR, 1,1-dioctadecyl-3,3,3,3 tetramethylindotricarbocyaine iodide; OVA, ovalbumin; PBS, phosphate-buffered saline; T$_H$, T helper.
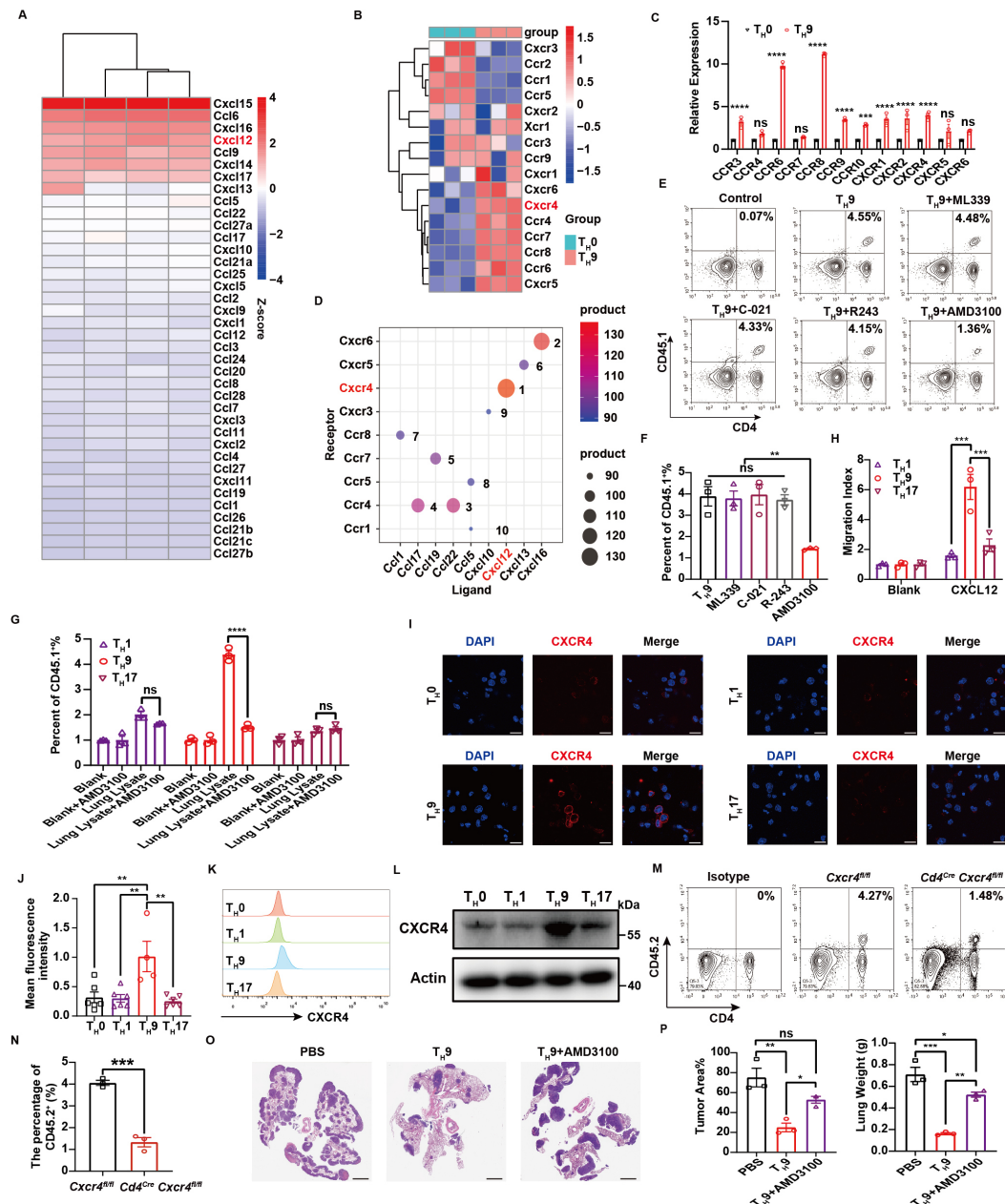
Figure 3 The CXCR4-CXCL12 axis mediates the lung tropism of T_H9 cells. (A) The expression of chemokines in normal lung tissue was analyzed from the GSE179554 data set. (B) Heat map of chemokine receptor genes in T_H0 and T_H9 cells. (C) Real-time PCR analysis of the expression of the chemokine receptors in T_H0 and T_H9 cells. (D) Bubble plot depicting ranked chemokine–chemokine receptors by the production of chemokines in lungs and chemokine receptors in T_H9 cells. (E and F) The representative density plot (E) and quantification (F) of CD45.1-T_H9 cells in the lungs 48 hours after intravenous injection of CD45.1-T_H9 cells into healthy CD45.2 mice. Healthy CD45.2 mice were received intraperitoneal (i.p.) injection of 1 mg kg^{-1} ML339, C-021, R243 and AMD3100, 24 hours before T cell transfer. (G) Migration index of T_H1, T_H9 and T_H17 cells with the presence or absence of lung lysate (100 μg/mL). The T_H cell subsets were pretreated with AMD3100 (5 μg/mL) or not. (H) Migration index of T_H1, T_H9 and T_H17 cells toward recombinant CXCL12 (10 ng/mL). (I) Immunofluorescence staining of CXCR4 in T_H1, T_H9 and T_H17 cells. Scale bar, 15 μm. (J) Statistical analysis of mean fluorescence intensity of CXCR4 in T_H1, T_H9 and T_H17 cells. (K) The intensity of CXCR4 expression detected in T_H0, T_H1, T_H9 and T_H17 cells by flow cytometry. (L) Western blotting analysis of CXCR4 protein levels in T_H0, T_H1, T_H9 and T_H17 cells. (M and N) The representative density plot (M) and statistical analysis (N) of CD45.2-T_H9 cells in the lung 48 hours after intravenous injection of CD45.2 WT derived T_H9 cells and CD45.2-$Cd4^{cre} Cxcr4^{flox/flox}$ derived T_H9 cells into healthy CD45.1 mice. (O) H&E staining of lungs bearing with K7M2-OVA tumor on day 14. The mice were intravenously injected with T_H9 cells or AMD3100 (5 μg/mL) pretreated T_H9 cells on day 5 and day 12. Scale bar, 2.5 mm. (P) Statistical analysis of tumor weight and tumor area corresponds to (O). Data were analyzed by one-way ANOVA test or unpaired t-test. Representative results from three independent experiments are shown (mean±SEM); n=3 in (C, E–H and M–P), n=4 or 6 in (I and J). ns denote no significant difference,*indicates $p<0.05$, **indicates $p<0.01$, ***indicates $p<0.001$, ****indicates $p<0.0001$. ANOVA, analysis of variance; DAPI, 4'6-diamidino-2-phenylindole; OVA, ovalbumin; PBS, phosphate-buffered saline; T_H, T helper; WT, wild-type.

after *Cxcr4* knockout (online supplemental figure S3F). To further confirm the role of the CXCR4-CXCL12 axis in the inhibitory effect of lung metastatic OS, tumor-bearing mice received a transfer of T_H9 cells pretreated by AMD3100. We found that AMD3100 greatly blunted the tumor inhibitory effect of T_H9 cells (figure 3O,P). However, AMD3100 pretreatment did not affect the antitumor effect of T_H1 and T_H17 cells (online supplemental figure S3G,H). Thus, these results indicate that the CXCR4-CXCL12 axis attracts T_H9 cells to the lungs.

ITCH regulates CXCR4 levels in T_H9 cells by ubiquitinating CXCR4

Then, we investigated how CXCR4 is upregulated in T_H9 cells. First, we compared the mRNA levels of *Cxcr4* among T_H0, T_H1, T_H9 and T_H17 cells. We found that *Cxcr4* expression was significantly upregulated in T_H9 cells compared with T_H0 cells, consistent with the bulk RNA sequencing of T_H0 and T_H9 cells mentioned in figure 3B. However, *Cxcr4* mRNA levels a T_H1, T_H9 and T_H17 cells showed no difference (figure 4A). In addition, we found that lysosome inhibitor chloroquine treatment led to comparable CXCR4 protein levels among T_H1, T_H9 and T_H17 cells (figure 4B). However, treatment with the proteasome inhibitor MG132 (Z-Leu-Leu-Leu-al) did not eliminate the differences in CXCR4 expression among the three subsets, as T_H9 cells continued to exhibit the highest CXCR4 levels (figure 4C). These results indicate that different CXCR4 protein levels among these T_H cell subsets were due to the post-translational modification. Consistently, previous studies reported CXCR4 protein levels were regulated by the process of ubiquitination and lysosome trafficking.[35 36] Thus, we detected the levels of ubiquitinated CXCR4 in T_H0, T_H1, T_H9 and T_H17 cells. Interestingly, T_H9 cells contained the lowest levels of ubiquitinated CXCR4 proteins (figure 4D). To find out the E3 ligase responsible for CXCR4 ubiquitination degradation, we overexpressed CXCR4 in 3T3 cells (figure 4E) and performed mass spectrum analysis to identify the E3 ligases pulled down by CXCR4. We identified 10 E3 ligases in 3T3 cells with empty vector or *Cxcr4* overexpression, among which ITCH was upregulated in CXCR4-overexpressing cells (figure 4F). ITCH was reported to degrade CXCR4 and prevent the formation of immune synapse required for T cell activation.[35 37] Consistently, ITCH was verified to be immunoprecipitated by CXCR4 (figure 4G). To confirm the function of ITCH on CXCR4 regulation in T_H9 cells, we silenced *Itch* and found increased CXCR4 proteins in T_H9 cells (figure 4H). Furthermore, ITCH overexpression markedly reduced CXCR4 proteins in T_H9 cells (figure 4I). These results indicate that ITCH is the E3 ligase responsible for CXCR4 ubiquitination degradation in T_H9 cells.

Subsequently, we determined that ITCH-mediated CXCR4 regulation affects the lung tropism of T_H9 cells. As presented in online supplemental figure S4 and figure 4J, we found that T_H9 cells with *Itch* silencing significantly increased the lung tropism of T_H9 cells, which was accompanied by enhanced antitumor effect of these T_H9 cells (figure 4K–M). Altogether, these results indicated that ITCH is functional in the lung tropism of T_H9 cells by regulating CXCR4.

Hyperactivation of NF-κB signaling in T_H9 cells inhibits ITCH function

Since ITCH regulates CXCR4 protein levels in T_H9 cells, we wondered whether different CXCR4 protein levels among T_H1, T_H9 and T_H17 cells are due to distinct ITCH expression among these T_H subsets. However, ITCH protein levels were similar among T_H0, T_H1, T_H9 and T_H17 cells (figure 5A). The ubiquitination activity of ITCH can be regulated by post-translational modification, especially Ser/Thr phosphorylation.[38 39] Therefore, we speculated the ubiquitination activity of ITCH is different among T_H cell subsets. As presented in figure 5B, we found increased Ser/Thr phosphorylation of ITCH in T_H9 cells compared with T_H1 and T_H17 cells (figure 5B). Previous studies unveiled that family tyrosine kinase (FYN) proto-oncogene, Src FYN, serum/glucocorticoid regulated kinase family member 3 (SGK3) and IKKs-mediated ITCH phosphorylation blunt ITCH's E3 ubiquitin ligase activity.[40–43] Thus, we detected the activation of FYN, SGK3 and IKKs in T_H9 cells, respectively. Our results reveal that, in comparison to T_H1 and T_H17 cells, T_H9 cells exhibit a significant upregulation of IKK phosphorylation levels, whereas the phosphorylation levels of SGK3 and FYN remain largely unchanged (figure 5C–E). IKKs are primarily responsible for the phosphorylation of IκB and activation of NF-κB signaling pathways. To determine the underlying mechanisms for increased Ser/Thr phosphorylation of ITCH in T_H9 cells, we detected the activation of NF-κB signaling pathways in T_H cell subsets. Expectedly, upstream signaling proteins of NF-κB, including p-IKKα/β and p- IκB, were activated at higher levels in T_H9 cells (figure 5E), which is consistent with a previous publication indicating that NF-κB activation is related to the hyperproliferative feature of T_H9 cells.[21] Subsequently, we conducted bulk RNA sequencing among T_H1, T_H9 and T_H17 cells to confirm the proliferation phenotype of T_H9 cells. We performed principal component analysis and found significant differences in the transcriptome profiles among the three groups (online supplemental figure S5A). Subsequently, differential expression analysis was conducted between T_H9 versus T_H1 and T_H9 versus T_H17, revealing that the RNA level of IL-9 was significantly upregulated in T_H9 cells, indicating successful induction of T_H9 cells. The differential expression analysis showed that compared with T_H1 cells, T_H9 cells had 683 upregulated genes and 781 downregulated genes, while compared with T_H17 cells, T_H9 cells had 402 upregulated genes and 665 downregulated genes (online supplemental figure S5B). We then performed gene ontology (GO) enrichment analysis on these differentially expressed genes and clustered the top 300 biological process terms. We found that terms related to T cell proliferation were significantly enriched
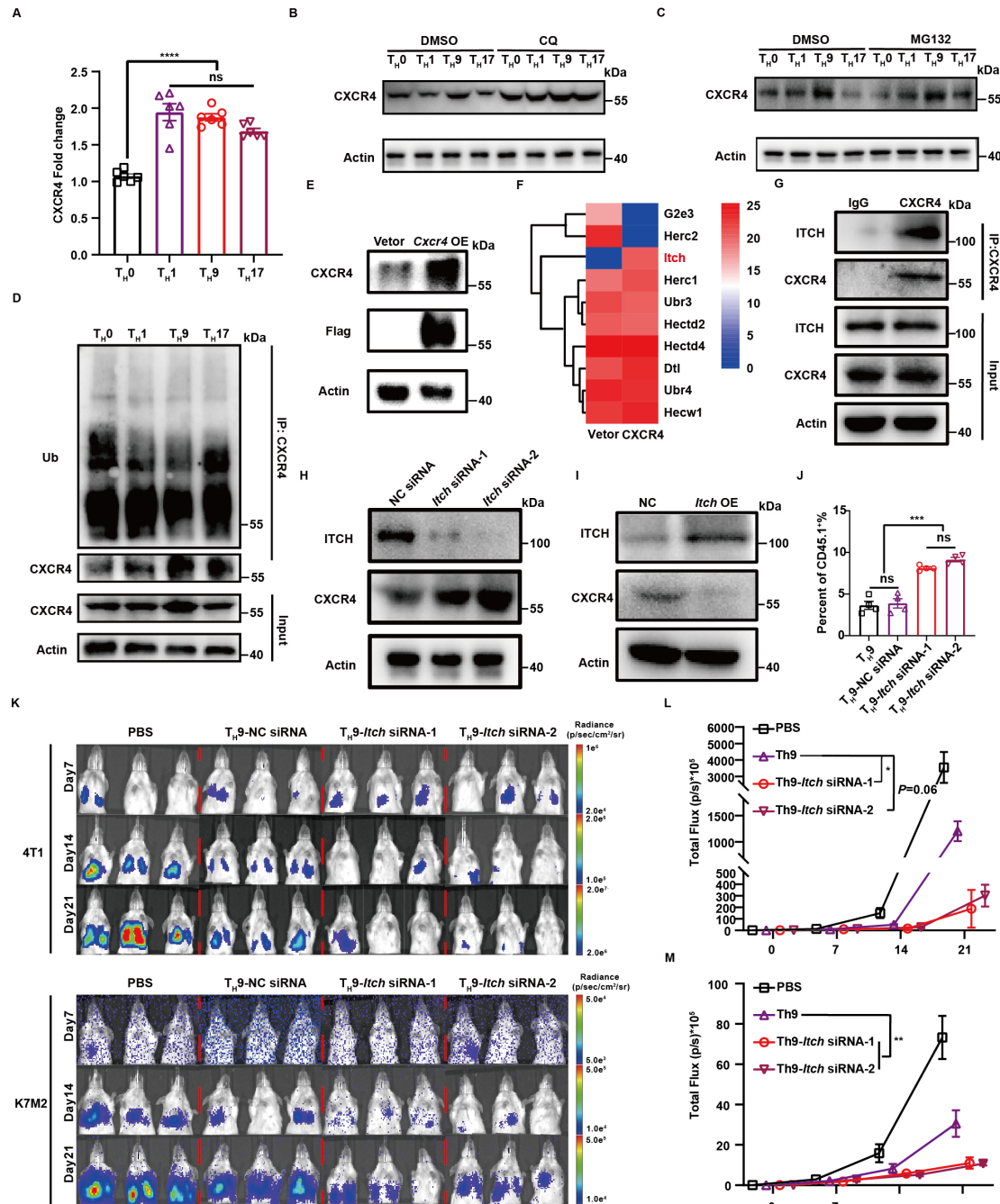
Figure 4 ITCH regulates the ubiquitination of CXCR4 in T_H9 cells. (A) Real-time PCR analysis of *Cxcr4* mRNA level in T_H0, T_H1, T_H9 and T_H17 cells. (B and C) Western blotting analysis of CXCR4 protein level in T_H9 cells stimulated with or without 10 µM CQ or 20 µM MG132 for 4 hours. (D) Immunoprecipitation analysis of ubiquitinated CXCR4 level in T_H0, T_H1, T_H9 and T_H17 cells. (E) Western blotting analysis of CXCR4 and Flag expression in 3T3 and 3T3 overexpressed with CXCR4. (F) Mass spectrum identified the E3 enzymes from proteins pulled down by CXCR4 among vector-3T3 and *cxcr4*-overexpression-3T3 samples. (G) Immunoprecipitation analysis of ITCH protein in T_H9 cells. (H) Western blotting analysis of CXCR4 protein level in T_H9 cells treated by negative control or *Itch*-siRNAs. (I) Western blotting analysis of CXCR4 protein level in T_H9 cells treated by negative control or *Itch*-OE retroviral. (J) Statistical analysis of flow cytometry was conducted on CD45.1-T_H9 cells in the lung 48 hours after intravenous injection of CD45.1-derived T_H9 cells treated with either negative control or *Itch*-siRNAs into healthy CD45.2 mice. (K) *In vivo* bioluminescence images of 4T1 or K7M2 tumor burden in the lungs on day 7, day 14 and day 21. The mice were treated with PBS or tumor-specific T_H9 treated with either negative control or *Itch*-siRNAs. (L and M) Statistical analysis of total flux in lungs bearing with 4T1 (L) or K7M2 (M) tumor. Data were analyzed by one-way ANOVA test or unpaired t-test. Representative results from three independent experiments are shown (mean±SEM); n=6 in (A), n=4 in (J), n=3 in (K). ns denote no significant difference, *indicates p<0.05, **indicates p<0.01, ***indicates p<0.001, ****indicates p<0.0001 (unpaired two-tailed Student's t-test). ANOVA, analysis of variance; CQ, chloroquine; DMSO, dimethyl sulfoxide; IgG, immunoglobulin G; mRNA, messenger RNA; NC, negative control; OE, overexpression; PBS, phosphate-buffered saline; siRNA, small interference RNA; T_H, T helper.
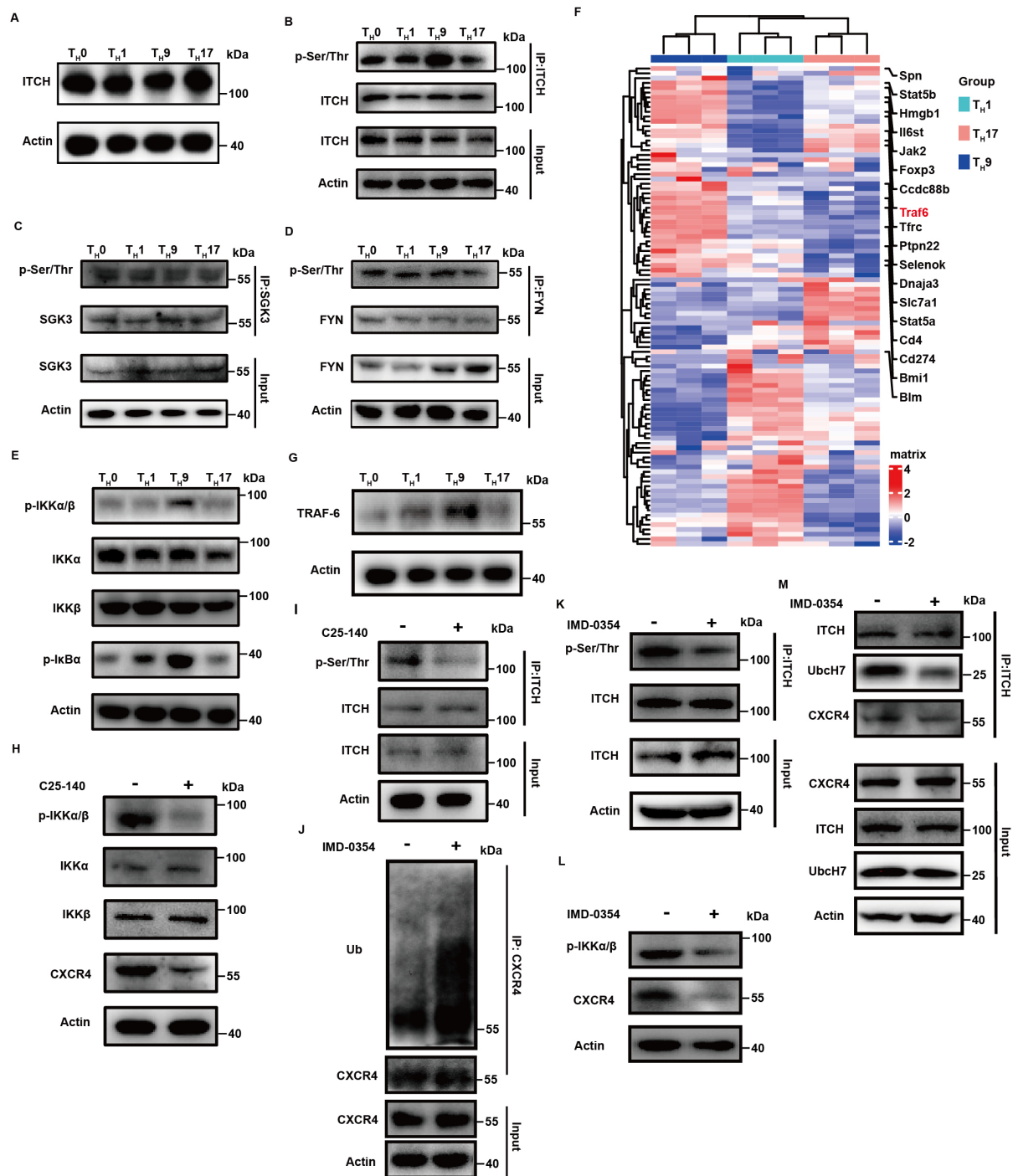
Figure 5 TRAF6 mediates IKKs phosphorylation and blunted ITCH activity in T_H9 cells. (A) Western blotting analysis of ITCH protein level in T_H0, T_H1, T_H9 and T_H17 cells. (B) Western blotting analysis of Ser/Thr phosphorylated ITCH protein level in T_H0, T_H1, T_H9 and T_H17 cells. (C and D) Western blotting analysis of phosphorylated SGK3 and FYN protein level in T_H0, T_H1, T_H9 and T_H17 cells. (E) Western blotting analysis of phosphorylated IKKα/β, IKKα, IKKβ and phosphorylated IκBα protein level in T_H0, T_H1, T_H9 and T_H17 cells. (F) Heatmap of the genes in the positive regulation of T cell proliferation gene set (GO:0042102) among T_H1, T_H9 and T_H17 cells. (G) Western blotting analysis of TRAF6 protein level in T_H0, T_H1, T_H9 and T_H17 cells. (H) Western blotting analysis of phosphorylated IKKα/β, IKKα, IKKβ and CXCR4 protein level in T_H9 cells treated with or without TRAF6 inhibitor, C25-140 (10 μM) for 2 hour. (I) Western blotting analysis of Ser/Thr phosphorylated ITCH protein level in T_H9 cells treated with or without TRAF6 inhibitor, C25-140 (10 μM) for 2 hours. (J) Immunoprecipitation analysis of ubiquitinated CXCR4 level in T_H9 cells treated with or without IKKs phosphorylation inhibitor, IMD-0354 (10 μM) for 24 hours. (K and L) Western blotting analysis of phosphorylated ITCH, CXCR4 and phosphorylated IKKα/β protein level in T_H9 cells treated with or without IKKs phosphorylation inhibitor, IMD-0354 (10 μM) for 24 hours. (M) Immunoprecipitation analysis of UbcH7 and CXCR4 levels in T_H9 cells treated with or without IKKs phosphorylation inhibitor, IMD-0354 (10 μM) for 24 hours. Representative results from three independent experiments are shown. FYN, family tyrosine kinase; IKK, inhibitor of nuclear factor kappa B kinase; SGK3, serum/glucocorticoid regulated kinase family member 3; T_H, T helper; TRAF6, tumor necrosis factor receptor associated factor 6.

in T_H9 cells (online supplemental figure S5C,D). Furthermore, we displayed a heatmap of the expression values of the positive regulation of T cell proliferation gene set (GO:0042102) among the three groups, which showed that a large number of genes involved in promoting T cell proliferation were upregulated in T_H9 cells (figure 5F). We further performed the gene set enrichment analysis (GSEA) analysis and enriched six activated and two suppressed pathways in T_H9 cells compared with T_H1 cells. Among the activated pathways, G2M checkpoint and TNF-α signaling *via* NF-κB pathways are associated with proliferation and enriched in T_H9 cells compared with T_H1 cells (online supplemental figure S5E). Similarly, Myc targets and TNF-α signaling *via* NF-κB signaling are enriched in T_H9 cells compared with T_H17 cells (online supplemental figure S5F). These results support that T_H9 cells possess a hyperproliferative feature and activation of NF-κB signaling. PU.1-mediated TRAF6 upregulation activated NF-κB signaling in T_H9 cells.[21] According to our result, *Traf6* was upregulated in T_H9 cells compared with T_H1 and T_H17 cells (figure 5F). We also detected higher TRAF6 protein levels in T_H9 cells than in T_H1 and T_H17 cells (figure 5G). Then, we inhibited TRAF6 activity with C25-140 in T_H9 cells and found that the phosphorylation of IKKs and ITCH was remarkably inhibited, along with reduced CXCR4 proteins (figure 5H,I). When the activity of IKKs was inhibited by its selective inhibitor IMD-0354, the ubiquitination level of CXCR4 was significantly enhanced (figure 5J). Correspondingly, we observed a reduction in the phosphorylation levels of ITCH, which paralleled the inhibition of IKKs activity, along with a notable decrease in the levels of CXCR4 (figure 5K,L). Perez *et al* reported that IKKs-driven phosphorylation of ITCH impedes its binding to the cognate E2 ubiquitin ligase UbcH7, rather than disrupting the interaction between ITCH and its targets.[40] Our experimental results further supported this notion. We found that when IKKs-mediated phosphorylation of ITCH was inhibited, the interaction between ITCH and CXCR4 remained unaffected, while the binding of ITCH to its E2 conjugating enzyme UbcH7 was significantly increased (figure 5M). Altogether, these results suggest that TRAF6-mediated IKKs activation impairs ITCH's E3 ligase activity, leading to reduced degradation of CXCR4 in T_H9 cells.
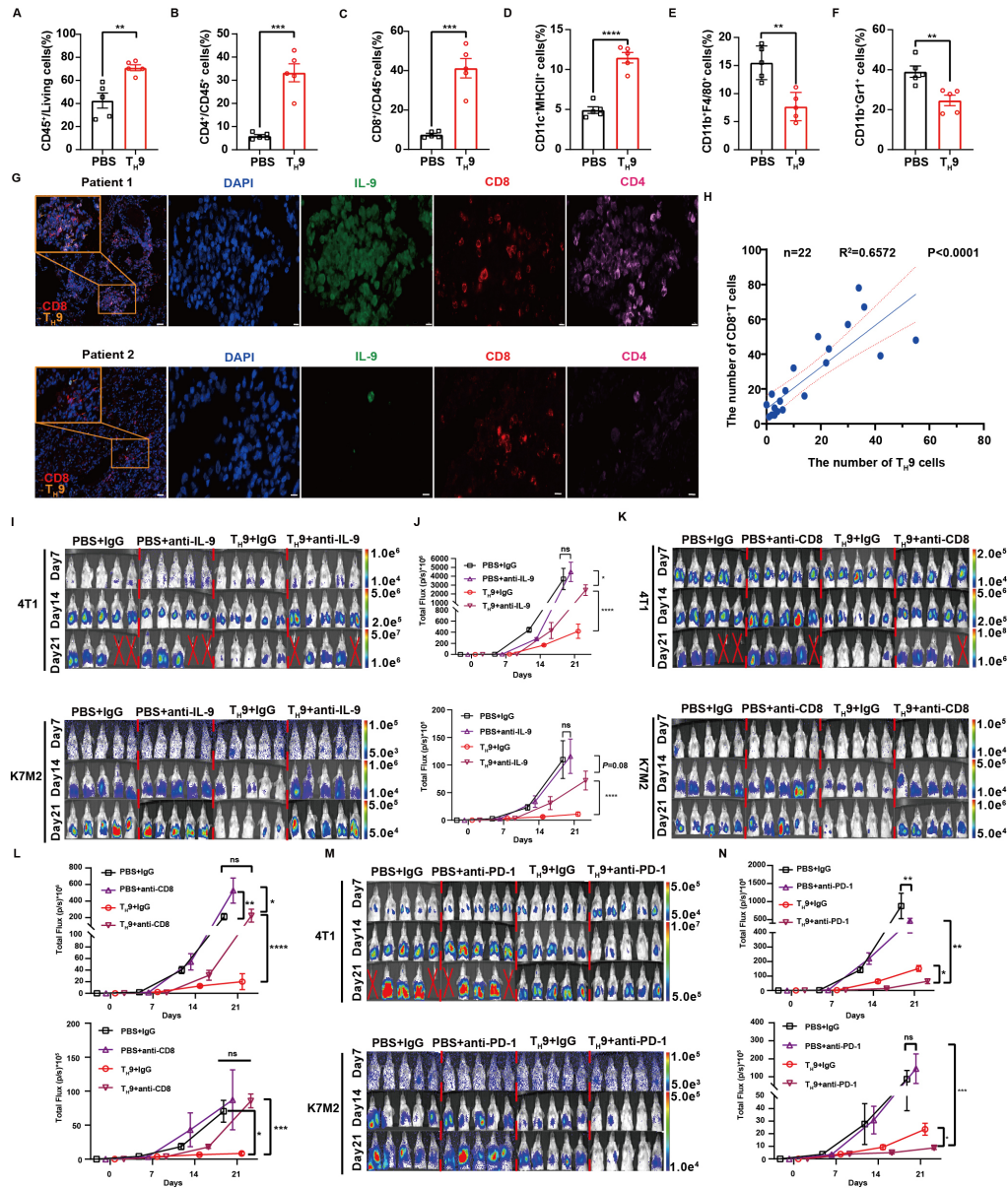
T_H9 cells effectively reshape the immune microenvironment of tumors and synergize with anti-PD-1 therapy

Finally, we sought to elucidate how T_H9 cells exert the antitumor effects in the lungs. K7M2-OVA lung tumor-bearing mice were transferred with T_H9-OVA cells. The infiltration of immune cells in lung tumors was then analyzed on day 14 after tumor inoculation. We observed significantly increased infiltration of $CD45^+$ leukocytes in lung tumors of mice with T_H9 cell transfusion (online supplemental figure S6A and figure 6A), as well as the increased proportion of $CD4^+$ T cells, $CD8^+$ T cells and dendritic cells (DCs) (online supplemental figure S6B–D and figure 6B–D). Furthermore, we found that the

proportion of immune suppressive leukocytes was substantially decreased, including tumor-associated macrophage (TAM) and myeloid-derived suppressor cells (MDSC) (online supplemental figure S6E,F and figure 6E,F), with unchanged natural killer cell proportion (online supplemental figure S6G). Similar results were obtained in 4T1-OVA lung tumor-bearing mice with T_H9 cell transfusion (online supplemental figure S6H-J). Subsequently, we collected paraffin-embedded specimens from lung lesions following surgical resection in 22 patients diagnosed with OS lung metastasis (online supplemental table 1). Immunofluorescence staining was conducted to evaluate the infiltration of $CD8^+$ T cells and T_H9 cells within these metastatic lesions. Immunofluorescence staining revealed that the patients with high numbers of $IL-9^+ CD4^+$ T cells often exhibited high numbers of $CD8^+$ T cells (figure 6G). Further analysis confirmed the positive correlation between the numbers of $CD8^+$ T cells and $IL-9^+ CD4^+$ T cells in the tumor tissues (figure 6H). Our previous work has demonstrated that the antitumor effects of T_H9 cells on OS rely on IL-9, and IL-9 influences the immune microenvironment of OS.[24] Consistently, we found that the blockade of IL-9 greatly abolished the inhibitory effect of T_H9 cells on the progression of lung OS and breast cancer (figure 6I,J). Importantly, the deletion of IL-9 did not entirely eliminate its tumor-inhibiting effects. Mice in the T_H9+anti-IL-9 group exhibited a lower lung tumor burden compared with those in the PBS or PBS+anti-IL-9 groups. This finding suggests that the therapeutic efficacy of T_H9 cells against tumors may not be wholly dependent on IL-9. Furthermore, several research teams have reported that T_H9 cells can exert antitumor effects through the action of IL-21.[28 44] Besides, $CD8^+$ T cell depletion confirmed that the antitumor effects of T_H9 cells relied on $CD8^+$ T cells (online supplemental figure S6K, figure 6K,L). The results indicate that the therapeutic efficacy of T_H9 cells in addressing lung metastases of OS and breast cancer primarily depends on the increased population of $CD8^+$ T cells following T_H9 cell infusion. Although it remains uncertain whether this enhancement arises from IL-9-mediated peripheral recruitment or an increase in $CD8^+$ T cell proliferation, it is clear that IL-9 plays, at least, a partial role in its antitumor effects.

Considering the established evidence from both our current study and prior research that T_H9 cell infusion can enhance immune cell infiltration, we propose that T_H9 cells may offer a significant advantage in "inflaming" cold tumors, thereby addressing the challenge of their unresponsiveness to immune checkpoint inhibitor therapy.[16 22 45] A recent investigation revealed a rise in T_H9 cell populations among patients with melanoma who responded positively to treatment with the anti-PD-1 agent nivolumab.[46] This finding strongly reinforces the potential benefits of combining T_H9 cell therapy with immune checkpoint inhibitor treatment. As shown in figure 6M,N, combined T_H9 cells adoptive transfer with PD-1 blockade further improved the therapeutic effects of T_H9 cells

Figure 6 T_H9 cells effectively reshape the immune microenvironment of tumors and synergize with anti-PD-1 therapy. Balb/c mice were challenged intravenously with 1×10^5 K7M2-OVA cells and received PBS or tumor-specific T_H9 cells (3×10^6) transfusion on day 5 and day 12. The tumor infiltration immune cells were analyzed on day 14. (A–F) The tumor infiltration immune cells of osteosarcoma treated with or without tumor-specific T_H9 cells. The statistical analysis of CD45^{+} T cells (A), CD4^{+} T cells (B), CD8^{+} T cells (C), DC cells (D), TAM (E) and MDSC (F). (G) Representative immunofluorescence staining of CD8^{+} T cells and IL-9^{+} CD4^{+} T cells in tumor tissues from patients with osteosarcoma lung metastases. Arrows indicate CD8^{+} T cells or IL-9^{+} CD4^{+} T cells. Markers: DAPI represents nuclear (pseudocolored blue), IL-9 (FITC, pseudocolored green), CD4 (CY5, pseudocolored pink) and CD8 (CY3, pseudocolored red). Scale bar, 10 µm. (H) Pearson's correlation between CD8^{+} and IL-9^{+}CD4^{+} T cells in tumor tissues of patients with osteosarcoma lung metastases (I and J) *In vivo* bioluminescence images (I) and statistical analysis (J) of K7M2-OVA and 4T1-OVA in the lungs on day 7, day 14 and day 21, treated with PBS or tumor-specific T_H9 on day 5, day 12 and day 19, with the intraperitoneal administration of IL-9 neutralizing antibody (100 µg) or IgG (100 µg) every 2 days since day 0. (K and L) *In vivo* bioluminescence images (K) and statistical analysis (L) of K7M2-OVA and 4T1-OVA in the lungs on day 7, day 14 and day 21, treated with PBS or tumor-specific T_H9 on day 5, day 12 and day 19, with the intraperitoneal administration of anti-CD8a antibody (100 µg) or IgG (100 µg) every 2 days since day 0. (M and N) *In vivo* bioluminescence images (M) and statistical analysis (N) of K7M2-OVA and 4T1-OVA in the lungs on day 7, day 14 and day 21, treated with PBS or tumor-specific T_H9 on day 5, day 12 and day 19, with the intraperitoneal administration of anti-PD-1 (40 µg) or IgG (40 µg) every 2 days since day 0. Data were analyzed by one-way ANOVA test, unpaired t-test or Spearman's rank-order correlation test. Representative results from three independent experiments are shown (mean±SEM); n=5 in all groups. ns denote no significant difference,*indicates p<0.05, **indicates p<0.01, ***indicates p<0.001, ****indicates p<0.0001 (unpaired two-tailed Student's t-test). ANOVA, analysis of variance; DAPI, 4'6-diamidino-2-phenylindole; FITC, fluorescein Isothiocyanate; IgG, immunoglobulin G; IL, interleukin; MDSC, myeloid-derived suppressor cell; OVA, ovalbumin; PBS, phosphate-buffered saline; PD-1, programmed cell death protein-1; TAM, tumor-associated macrophage; T_H, T helper.

on lung OS and breast cancer. In order to compare the effects of T_H9 cells combination therapy with anti-PD-1 on tumor immunity, we performed HE staining and CD45^{+} and CD8^{+} T cell staining to visualize the tumor-infiltrating immune cells (online supplemental figure S7). CD45^{+} and CD8^{+} T cell staining revealed that the combination of T_H9 cells and anti-PD-1 treatment further increased immune cell infiltration in tumors compared with monotherapies. These data indicate that T_H9 cells synergize with anti-PD-1 treatment in the lung OS and breast cancer models.

DISCUSSION

Although the antitumor effect of T_H9 cells has been preliminarily validated in some solid tumors and holds potential as an adoptive cell transfer therapy,[18 21 22 28 45 47 48] there remains little research regarding their efficacy in more challenging solid tumors. In this study, we found that T_H9 cells also exhibited certain therapeutic effects on cold tumors such as OS and TNBC in subcutaneous and *in situ* tumor mouse models, although their efficacy was comparable to that of T_H1 and T_H17 cells. However,

T_H9 cells demonstrated significant superiority over T_H1 and T_H17 cells in treating established OS and TNBC lung metastases. In this study, we revealed that T_H9 cells upregulate TRAF6 expression, leading to the phosphorylation of IKKs and then inhibiting the ubiquitination function of ITCH, resulting in reduced degradation of CXCR4 protein and its accumulation in T_H9 cells, which confers them with a lung-tropism phenotype and ultimately leads to the excellent therapeutic efficacy of T_H9 cells in the treatment of established OS and breast cancer lung metastases (figure 7). Our findings contribute to a better understanding of the characteristics of T_H9 cells and provide new insights for developing T_H9-based adoptive cell transfer therapy.

TRAF6, a crucial adaptor protein, is pivotal in transmitting signals from the TNF receptor superfamily and Toll-like receptors. TRAF6 activates the non-canonical NF-κB signaling and promotes the differentiation of T_H9 cells induced by OX40 (CD134) and glucocorticoid-induced TNF receptor-related protein.[18 49] Consistently, our findings align with previous reports indicating that T_H9 cells
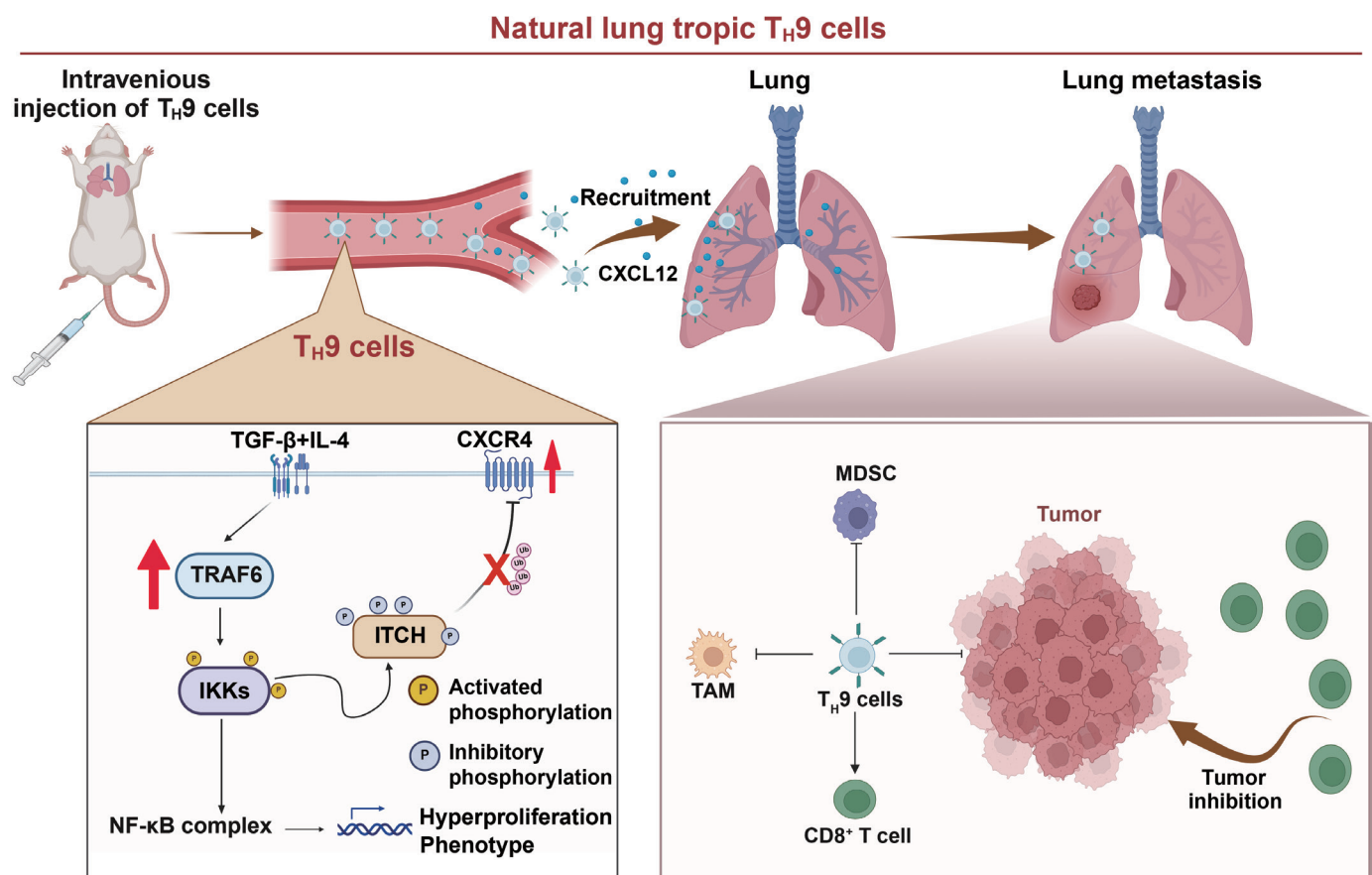
Figure 7 Working model of the mechanism of T_H9 cells' lung tropism and their antitumor effects. T_H9 cells upregulate TRAF6 expression to activate the NF-κB signaling pathway, which requires phosphorylation of IKKs and resulting in ITCH phosphorylation. Phosphorylation of ITCH by IKKs inhibits its E3 ligase activity, thereby attenuating CXCR4 degradation and ultimately resulting in its accumulation in T_H9 cells. Therefore, T_H9 cells preferentially accumulate in the lungs due to CXCL12 chemoattraction and exhibit lung tropism. In the setting of lung metastasis, transfusion of T_H9 cells inhibits tumor progression by enhancing the number of CD8^{+} T cells and ameliorating the immunosuppressive microenvironment with decreased TAM and MDSC. IKK, inhibitor of nuclear factor kappa B kinase; MDSC, myeloid-derived suppressor cell; TAM, tumor-associated macrophage; T_H, T helper; TRAF6, tumor necrosis factor receptor associated factor 6.

exhibit high expression of TRAF6, leading to the phosphorylation of IKKα/β and IκBα and activation of the NF-κB signaling pathway.[21] Lu *et al* have proposed that this phenomenon is driven by the T_H9 major transcription factor, PU.1, which sustains the highly proliferative phenotype of T_H9 cells. These results suggest that the activation of TRAF6 and NF-κB may be an inherent feature of T_H9 cells. To maintain the activation of the NF-κB signaling pathway, IKKs can phosphorylate ITCH, thereby attenuating its E3 ligase activity and further modulating the strength of the NF-κB signaling pathway.[40 41] At the same time, the E3 ubiquitin activity of ITCH is essential for CXCR4 degradation.[35 36] Thus, T_H9 cells have higher CXCR4 levels accumulated due to the attenuated degradation mediated by ITCH and, therefore, exhibit inherent lung tropism compared with T_H1 and T_H17 cells.

In addition, we found that T_H9 cells can effectively increase the proportion of CD45$^+$ and CD8$^+$ T cells in lung metastases of OS and breast cancer. This phenomenon is consistent with previous observations in other types of tumors.[16 45] Interestingly, we noticed a significant decrease in the population of TAM (CD11b$^+$ F4/80$^+$) and MDSC (CD11b$^+$ Gr1$^+$) in OS and TNBC lung metastases after T_H9 cell transfer. MDSC and TAM are prominent immunosuppressive cell populations observed in OS and TNBC.[50–55] They are widely acknowledged for their ability to facilitate tumor progression, metastasis, and association with unfavorable prognostic outcomes.[56 57] By administering T_H9 cell infusion, it is possible to attenuate the prevalence of these cell subsets, potentially through the augmentation of cytotoxic CD8$^+$ T cells and DCs, which exert inhibitory effects on tumor advancement. For example, studies have reported that chimeric antigen receptor T-Cell (CAR-T) therapy achieves immunomodulatory effects by heightening the homing capacity of cytotoxic T cells, consequently restraining the levels of inhibitory cell populations such as MDSC, thereby facilitating immune restructuring.[58 59] Additionally, tumor cells have been shown to drive the development and accumulation of MDSC and TAM through the secretion of cytokines and tumor-derived soluble factors.[60 61] Consequently, the inhibition of tumor progression by T_H9 cells may decrease the presence of MDSC and TAM within the tumor tissue.

Metastatic tumors are notoriously difficult to treat using conventional therapies. However, T_H9 cells' inherent preference for lung tissues may help overcome these barriers by selectively homing to the lung tissues. Once recruited, T_H9 cells can exert their recruiting ability to attract other immune cells, such as cytotoxic T lymphocytes and DC cells, to bolster the local immune response against tumor cells.[25 62] Besides, combining T_H9 cell therapy with PD-1 blockade produces enhanced antitumor effects, suggesting promising potential synergistic effects of T_H9 cells and immune checkpoint blockade therapy for cancer treatment. Recently, others have provided evidence that T_H9 cells or IL-9 can work in synergy with PD-1 blockade to induce a stronger antitumor immune response.[46 63–65]

Vinokurova and Apetoh concluded that PD-1 blockade triggers IL-9 responses in tumors, enhancing CD8$^+$ T cell functions or promoting immune cell infiltration. It is also likely that the PD-1 axis also regulates IL-9 production in T_H9 cells, amplifying the antitumor effects.[66] We speculate the synergistic effect of T_H9 cell-based adoptive cell therapy with immune checkpoint inhibitor therapy was attributed to the disruption of the balance between immunosuppressive cells and effector cells caused by T_H9 cells.

Despite accumulating evidence supporting the antitumor effects of T_H9 cells in solid tumors, their role in tumor immunity remains contentious due to protumor phenomena observed in hematological malignancies and non-hematological malignancies.[25–27 67] One potential explanation for this controversy is that IL-9, secreted by T_H9 cells, exerts proliferative and antiapoptotic effects on tumor cells in both hematological and non-hematological malignancies. IL-9 was initially characterized as a T cell growth factor and reported with pleiotropic functions in multiple cell types.[68 69] Furthermore, certain non-hematological tumor cells also express IL-9 receptors on their surface, which enables them to display proliferative and antiapoptotic traits in response to IL-9, as evidenced in A549 lung cancer cells, L1C2 cells, and hepatocellular carcinoma cells.[26 67] Consequently, the heterogeneity in IL-9R expression among solid tumor cells may represent a critical factor underlying the inconsistent effects observed with T_H9 cells. Furthermore, it is essential to evaluate the effects of IL-9 independently from those of T_H9 cells, as T_H9 cells not only produce IL-9 but also secrete IL-21. IL-21 is acknowledged for its antitumor properties, acting primarily by enhancing the effector functions of CD8$^+$ tumor-infiltrating lymphocytes.[28 70] Furthermore, the therapeutic potential of T_H9 cells against solid tumors is intricately linked to the heterogeneity of the tumor microenvironment. T_H9 cells achieve their antitumor effects by modulating the tumor microenvironment rather than solely targeting tumor cells directly.[25 69]

In conclusion, the lung tropism feature of T_H9 cells presents a promising avenue for treating cold tumors with lung metastasis. By leveraging their unique preference for lung tissues, T_H9 cells have the potential to enhance the recruitment and activation of immune cells within the tumor microenvironment, overcoming immunosuppression and improving antitumor immune responses. Further research and clinical studies are warranted to unlock the full potential of T_H9 cell-based therapies in the context of cold tumors, particularly those related to lung metastasis.

Author affiliations
[1]Department of Orthopedics, The Second Affiliated Hospital of Zhejiang University School of Medicine, Hangzhou, Zhejiang, People's Republic of China
[2]Orthopaedic Research Institute, Zhejiang University, Hangzhou, Zhejiang, People's Republic of China
[3]Key Laboratory of Motor System Disease Research and Precision Therapy of Zhejiang Province, Hangzhou, Zhejiang, People's Republic of China

[4]Department of Respiratory, The First Affiliated Hospital of Shandong First Medical University & Shandong Provincial Qianfoshan Hospital, Shandong Institute of Respiratory Diseases, Featured Laboratory of Respiratory Immunology and Regenerative Medicine in Universities of Shandong, Jinan Clinical Research Center for Respiratory Disease, Jinan, Shandong, People's Republic of China

[5]Department of Oncology, The Affiliated Cangnan Hospital of Wenzhou Medical University, Wenzhou, Zhejiang, People's Republic of China

[6]Eye Center, The Second Affiliated Hospital of Zhejiang University School of Medicine, Hangzhou, Zhejiang, People's Republic of China

[7]Zhejiang Provincial Key Lab of Ophthalmology, Hangzhou, Zhejiang, People's Republic of China

[8]Taizhou Hospital of Zhejiang Province affiliated to Wenzhou Medical University, Taizhou, Zhejiang, China

[9]Department of Respiratory and Critical Care Medicine, The First Affiliated Hospital of Wenzhou Medical University, Wenzhou, Zhejiang, China

[10]Institute of Immunology, Zhejiang University School of Medicine, Hangzhou, Zhejiang, China

Correction notice This article has been corrected since it was first published online. Figure 2 has been updated.

Contributors NL is responsible for the overall content as guarantor. TC, CQ, EY, and SW contributed equally to this work. Conceptualization: ZY, ZC, BL, and NL. Methodology: TC, CQ, and EY. Investigation: TC, CQ, SW, XJ, SL, and YX. Supervision: ZY, ZC, BL, and NL. Software: XW, XZ, and YF. Validation: HZ, WZ, and LJ. Analysis: TC, HL, HS, and ZW. Writing-original draft: TC. Writing—review and editing: CQ, TC, and LJ.

Competing interests None declared.

Patient consent for publication Not applicable.

Ethics approval This study involves human participants and was approved by Human Research Ethics Committee of the Second Affiliated Hospital, Zhejiang University College of Medicine, reference number: 2021-0179. Participants gave informed consent to participate in the study before taking part.

Provenance and peer review Not commissioned; externally peer reviewed.

Data availability statement Data are available upon reasonable request.

ORCID iD
Tao Chen http://orcid.org/0009-0004-4951-6283

REFERENCES

1 Altorki NK, Markowitz GJ, Gao D, *et al*. The lung microenvironment: an important regulator of tumour growth and metastasis. *Nat Rev Cancer* 2019;19:9–31.
2 Steeg PS. Targeting metastasis. *Nat Rev Cancer* 2016;16:201–18.
3 Ganesh K, Massagué J. Targeting metastatic cancer. *N Med* 2021;27:34–44.
4 Gerstberger S, Jiang Q, Ganesh K. Metastasis. *Cell* 2023;186:1564–79.
5 Minn AJ, Gupta GP, Siegel PM, *et al*. Genes that mediate breast cancer metastasis to lung. *Nat New Biol* 2005;436:518–24.
6 Gianferante DM, Mirabello L, Savage SA. Germline and somatic genetics of osteosarcoma - connecting aetiology, biology and therapy. *Nat Rev Endocrinol* 2017;13:480–91.
7 Fousek K, Ahmed N. The Evolution of T-cell Therapies for Solid Malignancies. *Clin Cancer Res* 2015;21:3384–92.
8 Newick K, O'Brien S, Moon E, *et al*. CAR T Cell Therapy for Solid Tumors. *Annu Rev Med* 2017;68:139–52.
9 Leon-Ferre RA, Goetz MP. Advances in systemic therapies for triple negative breast cancer. *BMJ* 2023;381:e071674.
10 Veldhoen M, Uyttenhove C, van Snick J, *et al*. Transforming growth factor-β "reprograms" the differentiation of T helper 2 cells and promotes an interleukin 9–producing subset. *Nat Immunol* 2008;9:1341–6.
11 Dardalhon V, Awasthi A, Kwon H, *et al*. IL-4 inhibits TGF-beta-induced Foxp3+ T cells and, together with TGF-beta, generates IL-9+ IL-10+ Foxp3(-) effector T cells. *Nat Immunol* 2008;9:1347–55.
12 Ouyang H, Shi Y, Su N, *et al*. Abnormality and significance of interleukin-9 and CD4(+)interleukin-9(+) T-cells in peripheral blood of patients with systemic lupus erythematosus. *Zhonghua Yi Xue Za Zhi* 2013;93:99–103.
13 Dantas AT, Marques CDL, da Rocha Junior LF, *et al*. Increased Serum Interleukin-9 Levels in Rheumatoid Arthritis and Systemic Lupus Erythematosus: Pathogenic Role or Just an Epiphenomenon? *Dis Markers* 2015;2015:519638.
14 Jäger A, Dardalhon V, Sobel RA, *et al*. Th1, Th17, and Th9 effector cells induce experimental autoimmune encephalomyelitis with different pathological phenotypes. *J Immunol* 2009;183:7169–77.
15 Fonseca-Camarillo G, Yamamoto-Furusho JK. Immunoregulatory Pathways Involved in Inflammatory Bowel Disease. *Inflamm Bowel Dis* 2015;21:2188–93.
16 Lu Y, Hong S, Li H, *et al*. Th9 cells promote antitumor immune responses in vivo. *J Clin Invest* 2012;122:4160–71.
17 Zhao Y, Chu X, Chen J, *et al*. Dectin-1-activated dendritic cells trigger potent antitumour immunity through the induction of Th9 cells. *Nat Commun* 2016;7:12368.
18 Kim I-K, Kim B-S, Koh C-H, *et al*. Glucocorticoid-induced tumor necrosis factor receptor-related protein co-stimulation facilitates tumor regression by inducing IL-9-producing helper T cells. *Nat Med* 2015;21:1010–7.
19 Kim I-K, Koh C-H, Jeon I, *et al*. GM-CSF Promotes Antitumor Immunity by Inducing Th9 Cell Responses. *Cancer Immunol Res* 2019;7:498–509.
20 Abdul-Wahid A, Cydzik M, Prodeus A, *et al*. Induction of antigen-specific TH 9 immunity accompanied by mast cell activation blocks tumor cell engraftment. *Int J Cancer* 2016;139:841–53.
21 Lu Y, Wang Q, Xue G, *et al*. Th9 Cells Represent a Unique Subset of CD4+ T Cells Endowed with the Ability to Eradicate Advanced Tumors. *Cancer Cell* 2018;33:1048–60.
22 Purwar R, Schlapbach C, Xiao S, *et al*. Robust tumor immunity to melanoma mediated by interleukin-9-producing T cells. *Nat Med* 2012;18:1248–53.
23 Das S, Surve V, Marathe S, *et al*. IL-9 Abrogates the Metastatic Potential of Breast Cancer by Controlling Extracellular Matrix Remodeling and Cellular Contractility. *J Immunol* 2021;206:2740–52.
24 Chen T, Xue Y, Wang S, *et al*. Enhancement of T cell infiltration via tumor-targeted Th9 cell delivery improves the efficacy of antitumor immunotherapy of solid tumors. *Bioact Mater* 2023;23:508–23.
25 Angkasekwinai P, Dong C. IL-9-producing T cells: potential players in allergy and cancer. *Nat Rev Immunol* 2021;21:37–48.
26 Ye Z-J, Zhou Q, Yin W, *et al*. Differentiation and immune regulation of IL-9-producing CD4+ T cells in malignant pleural effusion. *Am J Respir Crit Care Med* 2012;186:1168–79.
27 Salazar Y, Zheng X, Brunn D, *et al*. Microenvironmental Th9 and Th17 lymphocytes induce metastatic spreading in lung cancer. *J Clin Invest* 2020;130:3560–75.
28 Végran F, Berger H, Boidot R, *et al*. The transcription factor IRF1 dictates the IL-21-dependent anticancer functions of TH9 cells. *Nat Immunol* 2014;15:758–66.
29 Duan Q, Zhang H, Zheng J, *et al*. Turning Cold into Hot: Firing up the Tumor Microenvironment. *Trends Cancer* 2020;6:605–18.

30 Galon J, Bruni D. Approaches to treat immune hot, altered and cold tumours with combination immunotherapies. *Nat Rev Drug Discov* 2019;18:197–218.

31 Zlotnik A, Burkhardt AM, Homey B. Homeostatic chemokine receptors and organ-specific metastasis. *Nat Rev Immunol* 2011;11:597–606.

32 McCully ML, Kouzeli A, Moser B. Peripheral Tissue Chemokines: Homeostatic Control of Immune Surveillance T Cells. *Trends Immunol* 2018;39:734–47.

33 Janssens R, Struyf S, Proost P. The unique structural and functional features of CXCL12. *Cell Mol Immunol* 2018;15:299–311.

34 Floranović MP, Veličković LJ. Effect of CXCL12 and Its Receptors on Unpredictable Renal Cell Carcinoma. *Clin Genitourin Cancer* 2020;18:e337–42.

35 Marchese A, Raiborg C, Santini F, *et al*. The E3 ubiquitin ligase AIP4 mediates ubiquitination and sorting of the G protein-coupled receptor CXCR4. *Dev Cell* 2003;5:709–22.

36 Caballero A, Mahn SA, Ali MS, *et al*. Heterologous regulation of CXCR4 lysosomal trafficking. *J Biol Chem* 2019;294:8023–36.

37 Bhandari D, Robia SL, Marchese A. The E3 ubiquitin ligase atrophin interacting protein 4 binds directly to the chemokine receptor CXCR4 via a novel WW domain-mediated interaction. *Mol Biol Cell* 2009;20:1324–39.

38 Yin Q, Wyatt CJ, Han T, *et al*. ITCH as a potential therapeutic target in human cancers. *Semin Cancer Biol* 2020;67:117–30.

39 Aki D, Zhang W, Liu YC. The E3 ligase Itch in immune regulation and beyond. *Immunol Rev* 2015;266:6–26.

40 Perez JM, Chen Y, Xiao TS, *et al*. Phosphorylation of the E3 ubiquitin protein ligase ITCH diminishes binding to its cognate E2 ubiquitin ligase. *J Biol Chem* 2018;293:1100–5.

41 Perez JM, Chirieleison SM, Abbott DW. An IκB Kinase-Regulated Feedforward Circuit Prolongs Inflammation. *Cell Rep* 2015;12:537–44.

42 Yang C, Zhou W, Jeon MS, *et al*. Negative regulation of the E3 ubiquitin ligase itch via Fyn-mediated tyrosine phosphorylation. *Mol Cell* 2006;21:135–41.

43 Slagsvold T, Marchese A, Brech A, *et al*. CISK attenuates degradation of the chemokine receptor CXCR4 via the ubiquitin ligase AIP4. *EMBO J* 2006;25:3738–49.

44 You F-P, Zhang J, Cui T, *et al*. Th9 cells promote antitumor immunity via IL-9 and IL-21 and demonstrate atypical cytokine expression in breast cancer. *Int Immunopharmacol* 2017;52:163–7.

45 Schanz O, Cornez I, Yajnanarayana SP, *et al*. Tumor rejection in Cblb (-/-) mice depends on IL-9 and Th9 cells. *J Immunother Cancer* 2021;9.

46 Nonomura Y, Otsuka A, Nakashima C, *et al*. Peripheral blood Th9 cells are a possible pharmacodynamic biomarker of nivolumab treatment efficacy in metastatic melanoma patients. *Oncoimmunology* 2016;5:e1248327.

47 Rivera Vargas T, Cai Z, Shen Y, *et al*. Selective degradation of PU.1 during autophagy represses the differentiation and antitumour activity of TH9 cells. *Nat Commun* 2017;8:559.

48 Roy S, Rizvi ZA, Clarke AJ, *et al*. EGFR-HIF1α signaling positively regulates the differentiation of IL-9 producing T helper cells. *Nat Commun* 2021;12:3182.

49 Xiao X, Balasubramanian S, Liu W, *et al*. OX40 signaling favors the induction of T(H)9 cells and airway inflammation. *Nat Immunol* 2012;13:981–90.

50 Kansara M, Teng MW, Smyth MJ, *et al*. Translational biology of osteosarcoma. *Nat Rev Cancer* 2014;14:722–35.

51 Gill J, Gorlick R. Advancing therapy for osteosarcoma. *Nat Rev Clin Oncol* 2021;18:609–24.

52 Zhou Y, Yang D, Yang Q, *et al*. Single-cell RNA landscape of intratumoral heterogeneity and immunosuppressive microenvironment in advanced osteosarcoma. *Nat Commun* 2020;11:6322.

53 Bareche Y, Buisseret L, Gruosso T, *et al*. Unraveling Triple-Negative Breast Cancer Tumor Microenvironment Heterogeneity: Towards an Optimized Treatment Approach. *J Natl Cancer Inst* 2020;112:708–19.

54 Li W, Tanikawa T, Kryczek I, *et al*. Aerobic Glycolysis Controls Myeloid-Derived Suppressor Cells and Tumor Immunity via a Specific CEBPB Isoform in Triple-Negative Breast Cancer. *Cell Metab* 2018;28:87–103.

55 Kim IS, Gao Y, Welte T, *et al*. Immuno-subtyping of breast cancer reveals distinct myeloid cell profiles and immunotherapy resistance mechanisms. *Nat Cell Biol* 2019;21:1113–26.

56 van Vlerken-Ysla L, Tyurina YY, Kagan VE, *et al*. Functional states of myeloid cells in cancer. *Cancer Cell* 2023;41:490–504.

57 Barry ST, Gabrilovich DI, Sansom OJ, *et al*. Therapeutic targeting of tumour myeloid cells. *Nat Rev Cancer* 2023;23:216–37.

58 Sun R, Sun Y, Wu C, *et al*. CXCR4-modified CAR-T cells suppresses MDSCs recruitment via STAT3/NF-κB/SDF-1α axis to enhance efficacy against pancreatic cancer. *Mol Ther* 2023;31:3193–209.

59 Liu Y, Sun Y, Wang P, *et al*. FAP-targeted CAR-T suppresses MDSCs recruitment to improve the antitumor efficacy of claudin18.2-targeted CAR-T against pancreatic cancer. *J Transl Med* 2023;21:255.

60 Gabrilovich DI, Ostrand-Rosenberg S, Bronte V. Coordinated regulation of myeloid cells by tumours. *Nat Rev Immunol* 2012;12:253–68.

61 Yang L, Huang J, Ren X, *et al*. Abrogation of TGF beta signaling in mammary carcinomas recruits Gr-1+CD11b+ myeloid cells that promote metastasis. *Cancer Cell* 2008;13:23–35.

62 Speiser DE, Chijioke O, Schaeuble K, *et al*. CD4+ T cells in cancer. *Nat Cancer* 2023;4:317–29.

63 Feng Y, Yan S, Lam SK, *et al*. IL-9 stimulates an anti-tumor immune response and facilitates immune checkpoint blockade in the CMT167 mouse model. *Lung Cancer (Auckl)* 2022;174:14–26.

64 Fang H, Li R, Gu Y, *et al*. Intratumoral interleukin-9 delineates a distinct immunogenic class of gastric cancer patients with better prognosis and adjuvant chemotherapeutic response. *Oncoimmunology* 2020;9:1856468.

65 Wang C, Lu Y, Chen L, *et al*. Th9 cells are subjected to PD-1/PD-L1-mediated inhibition and are capable of promoting CD8 T cell expansion through IL-9R in colorectal cancer. *Int Immunopharmacol* 2020;78:106019.

66 Vinokurova D, Apetoh L. The Emerging Role of IL-9 in the Anticancer Effects of Anti-PD-1 Therapy. *Biomolecules* 2023;13:670.

67 Heim L, Yang Z, Tausche P, *et al*. IL-9 Producing Tumor-Infiltrating Lymphocytes and Treg Subsets Drive Immune Escape of Tumor Cells in Non-Small Cell Lung Cancer. *Front Immunol* 2022;13:859738.

68 Uyttenhove C, Simpson RJ, Van Snick J. Functional and structural characterization of P40, a mouse glycoprotein with T-cell growth factor activity. *Proc Natl Acad Sci U S A* 1988;85:6934–8.

69 Benoit-Lizon I, Apetoh L. Harnessing TH9 cells in cancer immunotherapy. *Semin Immunol* 2021;52:101477.

70 Cui C, Wang J, Fagerberg E, *et al*. Neoantigen-driven B cell and CD4 T follicular helper cell collaboration promotes anti-tumor CD8 T cell responses. *Cell* 2021;184:6101–18.